Stony Brook University

Ultrasonic Measurements of the Elastic Properties of Lanthanum/Cerium-based Bulk Metallic Glass and its Compression Behavior under High Pressure

A Thesis Presented

By

Xintong Qi

To

The Graduate School

in Partial Fulfillment of the

Requirements

For the Degree of

Master of Science

In

Materials Science and Engineering

Stony Brook University

May 2014

Stony Brook University

The Graduate School

Xintong Qi

We, the thesis committee for the above candidate for the

Master of Science degree, hereby recommend

acceptance of this thesis.

Dr. Baosheng Li – Thesis Advisor
Research Professor, Mineral Physics Institute

Dr. David O. Welch – Second Reader
Adjunct Professor, Department of Materials Science and Engineering

Dr. Dilip Gersappe -Third Reader
Associate Professor, Department of Materials Science and Engineering

This thesis is accepted by the Graduate School

Charles Taber
Dean of the Graduate School

Abstract of the Thesis

Ultrasonic Measurements of the Elastic Properties of Lanthanum/Cerium-based Bulk Metallic Glass and its Compression Behavior under High Pressure

by

Xintong Qi

Master of Science

in

Materials Science and Engineering

Stony Brook University

2014

Metallic glass, as a new member of glass family, has been at the cutting edge of material research for decades since it was first discovered in 1960. Its amorphous, densely packed microstructure makes it popular not only in industrial applications, but also in condensed matter physics. The elastic properties and their pressure dependence provide critical information about the bonding characteristics, microstructure and vibration features of metallic glasses. In this thesis, for the first time, the elastic wave velocities of $(La_{0.5}Ce_{0.5})_{64}Al_{16}Ni_5Cu_{15}$ bulk metallic glass are measured under high pressure up to 12.3 GPa using ultrasonic interferometry within a multi-anvil apparatus at room temperature. Analysis of acoustic and P-V data allows a direct determination of the elastic moduli such as the bulk modulus K, shear modulus G, Young's modulus E, and Poisson's ratio ν. Both longitudinal and shear modes exhibit softening behavior under low pressure similar to that of typical oxide glasses. This implies that Ce-based bulk metallic glass contains short-range covalent-like bonds. At higher pressure, discontinuities in bulk and shear moduli are observed at 5.9 GPa. The Debye temperature θ_D and Vickers hardness are also investigated to further understanding of its mechanical properties. All these results enable us to gain insight into the high pressure behavior and physical properties of bulk metallic glass, and also to further our understanding of the polyamorphism in Ce-based metallic glasses.

Table of Contents

List of Figures

List of Tables

List of Abbreviations

BMG	bulk metallic glass
GFA	glass forming ability
SRO	short-range ordering
MRO	medium-range ordering
XRD	x-ray diffraction
PEO	pulse echo overlap
LDA	low density amorphous
HDA	high density amorphous

Acknowledgments

I would like to express my very great appreciation to Dr. Baosheng Li, my thesis advisor, for his valuable and constructive suggestions during the planning and development of this research work. His willingness to give his time so generously has been very much appreciated.

I would like to offer my special thanks to Dr. David O. Welch for being in my committee member, his encouragement and useful comments on this thesis.

I would like to thank Dr. Dilip Gersappe for being in my committee member and his help on my research project.

My sincere thanks also go to Dr. Robert C. Liebermann, for his enthusiasm, immense knowledge and support in all stages of this thesis. His attitude to research inspired me to continue to a Ph.D program.

In addition, I would like to thank my colleagues: Dr. Yongtao Zou, Dr. Ying Li, Xuebing Wang, and Ting Chen for their great help in doing the experiments at the High Pressure Lab. Without their patience, it would not be a successful project.

I would like to thank Mineral Physics Institute, Department of Geosciences and Department of Materials Science and Engineering, for offering me good academic atmosphere and studying environment. Also, I would like to thank for financial support from DOE Grants No. DE-NA0001815.

Last, but not the least, I would like to thank my parents, Yuhua Li and Junjie Qi for always having faith in me, for their continuous love and many years of support during my studies.

Chapter1 Introduction

1.1 Developments of metallic glasses

"In condensed matter physics, an amorphous or non-crystalline solid is a solid that lacks the long-range order characteristic of a crystal. Amorphous metals, which are different from most metals with a highly ordered arrangement of atoms, are non-crystalline."[1] Materials in which such a disordered structure is produced directly from the liquid state during cooling are called "glasses", and so amorphous metals are commonly referred to as "metallic glasses" or "glassy metals".

In early days, it was thought impracticable to cool metals into a glassy state, because they are easily to crystallize. In1960 the first metallic glass of $Au_{75}Si_{25}$ was discovered by Duwez and co-workers at Caltech, USA. [2]. They developed the rapid quenching techniques to form non-crystalline structure in gold-silicon alloys at very high rates, 10^5-10^6 K/s. In 1969, Chen and Turnbull formed amorphous spheres of ternary Pd-M-Si (with M=Ag, Cu or Au) at cooling rates of 10^2 K/s to 10^3 K/s. [3] The alloy $Pd_{77.5}Cu_6Si_{16.5}$ could be made into a glass state with a diameter of 0.5mm and the glass-liquid transition was convincingly demonstrated. In some Pd-Cu-Si and Pd-Ag-Si alloys, the supercooled liquid range (between the crystallization and glass transition temperatures) was extended to 40K, which enabled the first detailed studies of crystallization in metallic glasses. In 1974, Chen investigated on Pd-T-P alloys (T=Ni, Co, Fe) systematically and obtained a critical casting thickness of 1mm in these alloys. [4] If one defines the millimeter scale as "bulk", this amorphous Pd-Cu-Si alloy could be considered to be the first bulk metallic glass. In 1982, a slightly greater thickness of approximately 1.5mm in $Au_{55}Pb_{22.5}Sb_{22.5}$ composition was obtained by M.C Lee et al. [5] In the early 1980s, the Turnbull's group studied Pd-Ni-P alloys and they successfully produced glassy ingots of $Pd_{40}Ni_{40}P_{20}$ with diameters of 5mm [6] and in 1984, they extended the critical casting diameter to 10mm by processing the Pd-Ni-P melt in a molten flux of dehydrated boron oxide.[7] At that time, however, the high cost of Pd metal limited its development and people did not recognize the engineering application potential of BMG either.

In the late 1980s, Inoue et al. in Tohoku University of Japan systematically investigated ternary alloys of rare-earth materials with Al and ferrous metals.[8][9] While studying rapid solidification in these systems, extraordinary glass-forming ability (GFA) in La-Al-Ni and La-

Al-Cu alloys was observed. [8] They obtained fully glassy cylindrical samples with diameters of up to 5mm or sheets with similar thicknesses by casting $La_{55}Al_{25}Ni_{20}$ into water-cooling Cu molds. Based on this work, the researchers studied similar quaternary and quinary materials (e.g. La-Al-Cu-Ni and La-Al-Cu-Ni-Co BMGs) and developed alloys that formed glass at cooling rates under 100 K/s with critical casting thickness reaching toward 1 cm. [9] In 1991, glassy Mg-Cu-Y and Mg-Ni-Y alloys with the largest glass-formation ability obtained in $Mg_{65}Cu_{25}Y_{10}$ was developed by the same group.[10] In the same year, the Inoue's group found amorphous Zr-Al-Tm (Tm=Co, Ni, Cu) alloys having a high glass-forming ability and stability by melt spinning. [11] The supercooled liquid region has been extended to 127 K for the alloy $Zr_{65}Al_{7.5}Ni_{10}Cu_{17.5}$ with a critical casting thickness of 15mm, which was believed to be the largest in metallic amorphous materials reported for the time. These multicomponent BMGs demonstrated that bulk glass-formation was far more ubiquitous than previously thought and not confined to Pd-based alloys.

With the development of these alloys, metallic glasses have attracted increasing attention not only because of their fundamental scientific importance, but also their potential for engineering applications. Building on the Inoue work, Johnson and his co-workers from Caltech developed a family of ternary, quinary and high-order glass-formers based on higher-order alloys of Zr, Ti, Cu, Ni and Be (also combined with other transition metals) [12-14]. In 1993, Johnson and Peker designed the quinary glassy alloy $Zr_{41.2}Ti_{13.8}Cu_{12.5}Ni_{10.0}Be_{22.5}$, as part of a US Department of Energy and NASA funded project to develop new aerospace materials. With critical casting thickness of several centimeters, the alloy became known as Vitreloy 1 (Vit1), the first commercial BMG. [15] The alloys were cast in Cu-mold in the form of fully glassy rods with diameters ranging up to 5-10 cm. The formation of these BMGs requires no fluxing or special processing treatment and can obtain bulk glass by conventional metallurgical casting methods. Its glass-forming ability and processability are comparable with those of many silicate glasses. This finding makes it possible to process metallic glasses by common methods in a foundry. [16] In 1997, the Inoue group developed $Pd_{40}Cu_{30}Ni_{10}P_{20}$ bulk amorphous alloy in cylindrical form of 72 mm in diameter. The Pd-Cu-Ni-P family is the metallic system with the highest glass-forming ability known to date. [17] In 2012, the world's biggest glassy alloy, $Pd_{42.5}Cu_{30}Ni_{7.5}P_{20}$ with a diameter of 80mm was successfully discovered by Nishiyama. [18] Table 1.1 lists the typical BMG systems and the year in which they were first reported. Ever since the discovery of

metallic glasses by Duwez and coworkers, this field is progressing at a fast pace and has attracted intense research interest in fundamental studies as well as technological advances. For the fundamental aspects, the extraordinary glass-forming ability and high stability of these materials have opened the opportunity to study the glass transition, crystal nucleation, growth kinetics and thermodynamic properties over the entire range of the undercooled liquid. For the functional aspects, these metallic glasses, with good glass-forming ability, have been found to display many excellent properties, which encouraged a wider variety of applications such as magnetic sensing, chemical and structural use. [19][20]

Table 1.1 Typical bulk glassy alloy systems reported up to date together with the calendar years when the first paper of patent of each alloy system was published. [21]

Non-ferromagnetic alloy systems	**Year**	**Ferromagnetic alloy systems**	**Year**
Mg–Ln–M (Ln = lanthanide metal, M = Ni, Cu, Zn)	1988	Fe–(Al,Ga)–(P,C,B,Si,Ge)	1995
Ln–Al–TM (TM = Fe, Co, Ni, Cu)	1989	Fe–(Nb,Mo)–(Al,Ga)–(P,B,Si)	1995
Ln–Ga–TM	1989	Co–(Al,Ga)–(P,B,Si)	1996
Zr–Al–TM	1990	Fe–(Zr,Hf,Nb)–B	1996
Zr–Ln–Al–TM	1992	Co–(Zr,Hf,Nb)–B	1996
Ti–Zr–TM	1993	Fe–Co–Ln–B	1998
Zr–Ti–TM–Be	1993	Fe–Ga–(Cr,Mo)–(P,C,B)	1999
Zr–(Ti,Nb,Pd)–Al–TM	1995	Fe–(Cr,Mo)–(C,B)	1999
Pd–Cu–Ni–P	1996	Ni–(Nb,Cr,Mo)–(P,B)	1999
Pd–Ni–Fe–P	1996	Co–Ta–B	1999
Ti–Ni–Cu–Sn	1998	Fe–Ga–(P,B)	2000
Ca–Cu–Ag–Mg	2000	Ni–Zr–Ti–Sn–Si	2001
Cu–Zr, Cu–Hf	2001	Ni–(Nb,Ta)–Zr–Ti	2002
Cu–(Zr,Hf)–Ti	2001	Fe–Si–B–Nb	2002
Cu–(Zr,Hf)–Al	2003	Co–Fe–Si–B–Nb	2002
Cu–(Zr,Hf)–Al–(Ag,Pd)	2004	Ni–Nb–Sn	2003
Pt–Cu–Ni–P	2004	Co–Fe–Ta–B–Si	2003

Ti–Cu–(Zr,Hf)–(Co,Ni)	2004	Ni–Pd–P	2004
Au–Ag–Pd–Cu–Si	2005	Fe–(Cr,Mo)–(C,B)–Ln (Ln = Y, Er, Tm)	2004
Ce–Cu–Al–Si–Fe	2005	Co–(Cr,Mo)–(C,B)–Ln (Ln = Y, Tm)	2005
Cu–(Zr,Hf)–Ag	2005	Ni–(Nb,Ta)–Ti–Zr–Pd	2006
Pd–Pt–Cu–P	2007	Ni–Pd–P–B	2009
Zr–Cu–Al–Ag–Pd	2007	Fe–(Nb,Cr)–(P,B,Si)	2010
Ti–Zr–Cu–Pd	2007		
Ti–Zr–Cu–Pd–Sn	2007		

1.2 Structure of bulk metallic glasses

The atomic structures of metallic glasses were first thought to be similar to or even the same as the atomic structures of those metallic liquids, because the most appropriate compositions for glass formation are those stabilizing liquid phase relative to crystalline phases. It is known that pure crystalline metals have dense packing, such as in face-centered cubic (fcc) and hexagonal close-packed (hcp) lattices. Upon melting, the density of metallic liquids only decreases by a few percent, indicating that those liquids are still rather dense. The most widely appreciated structure model for metallic glasses at that time was Bernal's dense random packing (DRP) of hard spheres (DRPHS) model. [22] He assumed that the glass was a frozen metallic liquid and the atoms in metals were approximated as hard spheres. The atomic arrangement was considered as a purely geometrical sphere packing. Bernal's idea can result in a satisfactory model for monatomic metals and alloys in which constituent species have comparable atomic sizes. However, it does not provide insight into the short-range and medium-range ordering (SRO and MRO, respectively) observed in real, multicomponent glassy system, and the effect of chemical interaction between atoms, especially in metal-metalloid-based alloys, was not taken into account. [23] Considering this, Gaskell gave a stereochemically defined model that guaranteed that the local unit with nearest neighbors in amorphous metal-metalloid alloys had the same type of structure and composition as their crystalline compounds. [24] However, this model has not been proven to be correct for metal-metal-based metallic glasses. As an alternative model for

dense packing, a closely packed icosahedral atomic arrangement has been widely considered to be a possible structural unit of BMGs. A number of simulations and experimental observations have suggested that the icosahedron is an energetically favorable atomic structure in some metal-metal-based metallic glasses. [25-27]

Recently, Miracle [28][29] described a structural model for metallic glasses that extends well beyond the nearest-neighbor shell based on a new sphere packing scheme - the efficient filling of space by solute-centered clusters. An extended structure is produced by idealizing these clusters as spheres and efficiently packing these sphere-like clusters in fcc or hcp configurations to fill the three-dimensional space. Because of the internal strains, the order of the cluster-forming solutes cannot extend beyond a few clusters diameters, so that long-range order in cluster packing is degraded. Adjacent clusters share solvent atoms in common faces, edges or vertices. There is no orientational order among the clusters, so that the solvent atoms occupy random positions in this structure. This provides an important distinction from the icosahedral glass model proposed for quasicrystalline structures. Fig.1.1 illustrates a typical dense cluster-packing structure thus comprises interpenetrating arrays of efficiently packed solute-centered clusters.

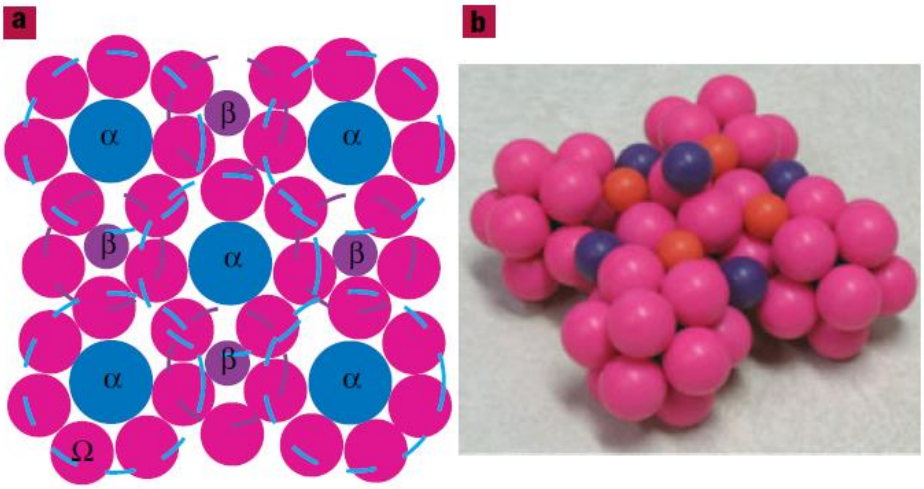

Fig. 1.1. Illustrations of portions of a single cluster unit cell for the dense cluster packing model.[29]

On the basis of experimental measurements and computational simulations, Sheng et al. [30] proposed an alternative cluster-packing scheme to resolve the atomic-level structure of

amorphous alloys. By analyzing a range of model binary systems that involve different chemistry and atomic size ratios, they elucidated the different types of SRO as well as the nature of the MRO. Their results suggest that icosahedral fivefold packing is a more realistic ordering pattern for SRO cluster-cluster connection in metallic glasses (Fig 1.2) than are fcc or hcp cluster packing.

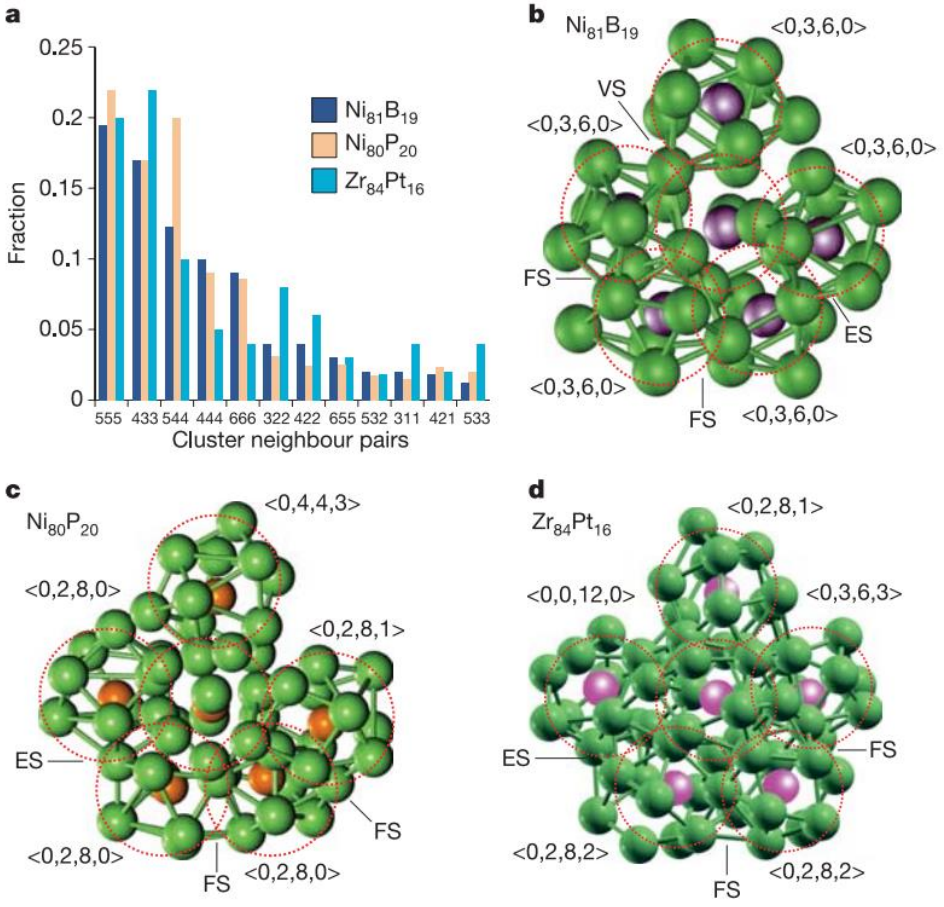

Fig. 1.2.(a) A cluster common-neighbor analysis showing that the local clusters in the metallic glasses exhibit icosahedral-type ordering. (b–d) The typical cluster connections, exhibiting fivefold symmetry, are detailed for (b) $Ni_{81}B_{19}$, (c) $Ni_{80}P_{20}$, and (d) $Zr_{84}Pt_{16}$. For each local cluster, the Voronoi index is given to indicate its identity. FS, ES, and $_{VS}$ denote face sharing, edge sharing, and vertex sharing, respectively. The red dashed circles delineate the clusters and suggest the quasi-equivalence of the clusters. For clarity, the bonds for the center clusters are not connected. [30]

1.3 Elastic properties of bulk metallic glasses and effects of high pressure

The study of the elastic properties and their temperature and/or pressure dependences of metallic glasses can provide critical information about the bonding characteristics, microstructure and vibration characteristics. [31] The equation of state (EOS) of a solid plays an important role in condensed matter physics, and the EOS of crystalline solids has been a long-standing, extensively studied topic. [32] Metallic glassy alloys are normally regarded as elastically isotropic solid, which makes them suitable for measurements of elastic wave propagation. For many years, however, the very high cooling rate (>10^5 K/s) of metallic glasses limits their geometry to very thin ribbons or wires, which makes it difficult to study the intrinsic nature of the glass and glass transition, as well as the establishment of EOS. The experimental data about acoustic and elastic properties in the metallic glasses are scarce due to the lack of bulk specimens.

The preparation of metallic glasses in bulk form makes the accurate study of their elastic properties using ultrasonic techniques possible. With the recent development of a variety of metallic glasses which readily form bulk glass, a considerable amount of data on their elastic and acoustic properties has been obtained. For example, the values of density, longitudinal velocity V_p and transverse velocity V_s of $Zr_{41}Ti_{14}Cu_{12.5}Ni_{10}Be_{22.5}$ BMG (Vit1) at ambient condition are 6.125 g/cm3, 5.17 km/s and 2.47 km/s, respectively. The Young's modulus (E), shear modulus (G), bulk modulus (K), Poisson's ratio (v) and Debye temperature (θ_D) of Vit1 calculated from the acoustic data are 101.2 GPa, 37.4GPa, 114.1 GPa, 0.35 and 326.8K, respectively. [33] In recent years, elastic data for almost all the known bulk metallic glasses have been obtained by using ultrasonic or other methods, including date for Zr-, Pd-, Pt-, Au-, Cu,Zr-, Cu-, Fe-, Mg-, Ni-, Ti-, Hf-, W-, Ta-, Ca-, Sr-, Ca,Li-, Ca,Yb-, Zn-, Sc-, Y-, La-, Nd-, Ce-, Ho-, Sm-, Er-, Gd-, Tb-, Dy-, Tm-, Lu-, Yb- and Pr-based BMG materials and hundreds of compositions. [34]

With the development of high pressure techniques, pressure is becoming an important processing variable just like that of temperature or chemical composition for condensed phases. High pressure, which can cause a large change of atom spacing, chemical bonding and Gibbs free energy, has been found to be a powerful tool for investigating the microstructure and local atomic rearrangement in bulk metallic glasses.

The pressure dependence of the structural and physical properties of the bulk metallic glasses can be accurately investigated by the ultrasonic method. [35] The pressure dependence of acoustic velocities can provide critical information on the microstructural, elastic and thermal characteristics, equation of state of glassy materials. Taking the typical $Zr_{41}Ti_{14}Cu_{12.5}Ni_{10}Be_{22.5}$ BMG (Vit1) as an example, the pressure dependence of V_p and V_s is shown in Fig. 1.3. The data of V_p and V_s are reproducible and show no measurable hysteresis effects in the pressure loading and release cycle, and there are no observable permanent changes in acoustic velocities up to 2.0 GPa. The corresponding pressure dependence of elastic constants Y (Y=E, G, K, ν) calculated from the velocities for Vit1 is shown in Fig.1.4.

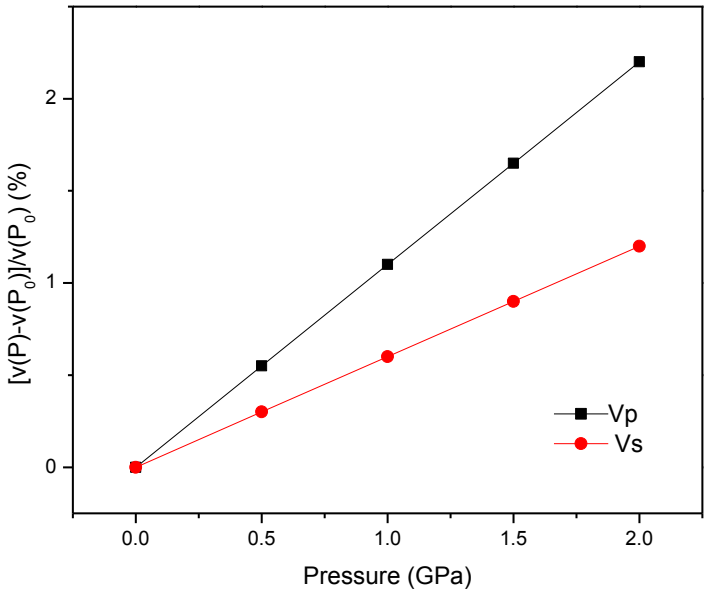

Fig. 1.3. The variation of longitudinal and transverse velocities ($V=V_p$, V_s) of the $Zr_{41}Ti_{14}Cu_{12.5}Ni_{10}Be_{22.5}$ BMG upon pressure at room temperature. V is normalized by V_0 (P) at ambient pressure P_0. [35]

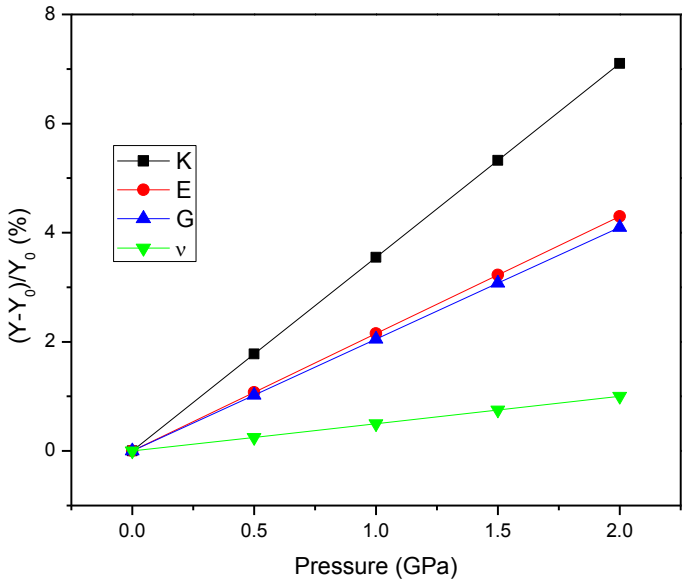

Fig. 1.4. The variation of elastic constants Y of the $Zr_{41}Ti_{14}Cu_{12.5}Ni_{10}Be_{22.5}$ BMG (Y=E, G, K, ν) with pressure, Y is normalized by $\Delta Y/Y_0 = (Y-Y_0)/Y_0$, where Y_0 is a normal modulus at P_0. [35]

As shown in Fig. 1.4, the pressure derivatives of E, G and K of BMGs are positive, showing that the BMGs stiffen under hydrostatic pressure. In contrast to BMGs, however, the V_p and V_s of the typical silicate Ti-glass decrease with increasing P, and the pressure derivatives of E, G and K are negative, indicating pressure induced acoustic mode softening.[36] The pressure dependence of elastic constants of a series of different BMGs has been systematically studied and similar change tendencies have been found. [34]

The only known exception so far is Ce-based BMGs. The Ce-based BMGs show unusual response of acoustic and elastic properties to hydrostatic pressure. In Fig.1.5, the pressure variations of ρ, V_p and V_s for a $Ce_{70}Al_{10}Ni_{10}Cu_{10}$ BMG at room temperature up to 0.5 GPa are shown. The acoustic velocities decrease with the increase of pressure. This is markedly different from other BMGs but rather similar to nonmetallic glasses, at least in this pressure range. Figure 1.6 presents the pressure dependence of the elastic constants compared with that of Vit1. Apparently, the Ce-based BMG exhibits much larger and different variations of ρ, V_p, K and ν than those of Vit1, strongly suggesting that the Ce-based BMG has a unique structure that is quite different from those of other BMGs. [37] Actually, an apparent amorphous to amorphous

phase transition indeed has been reported in Ce-based metallic glasses. [38] The transformation of a low-density glass state to a high-density glass state is attributed to the interaction of the strongly correlated 4f-electrons and their delocalization under pressure, which results in bond shortening. In a LaCe-based BMG, an unusual change in the compressibility at about 14 GPa, suggestive of polyamorphism, is also found. [39] All these results have implications for the understanding of the microstructure of metallic glass.

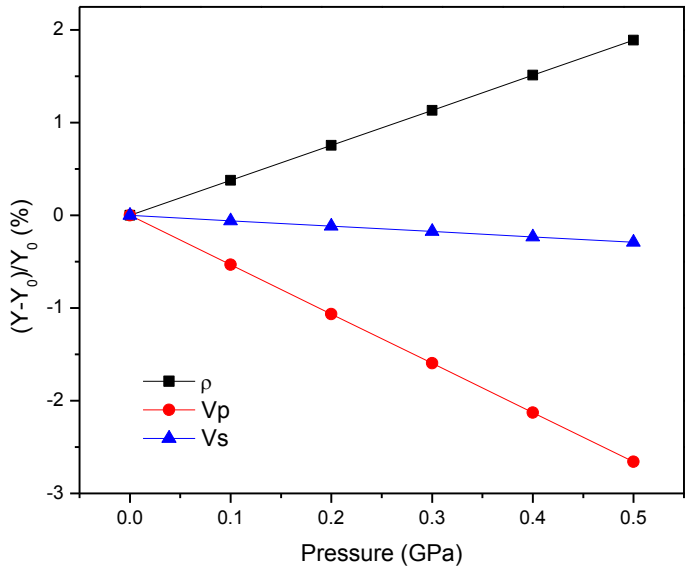

Fig. 1.5. Relative variations $\Delta Y(P)/Y(P_0)= [Y(P)-Y(P_0)]/Y(P_0)$ of ρ, V_p and V_s with pressure up to 0.5 GPa for the $Ce_{70}Al_{10}Ni_{10}Cu_{10}$ BMG at room temperature. P_0 is the ambient pressure. [37]

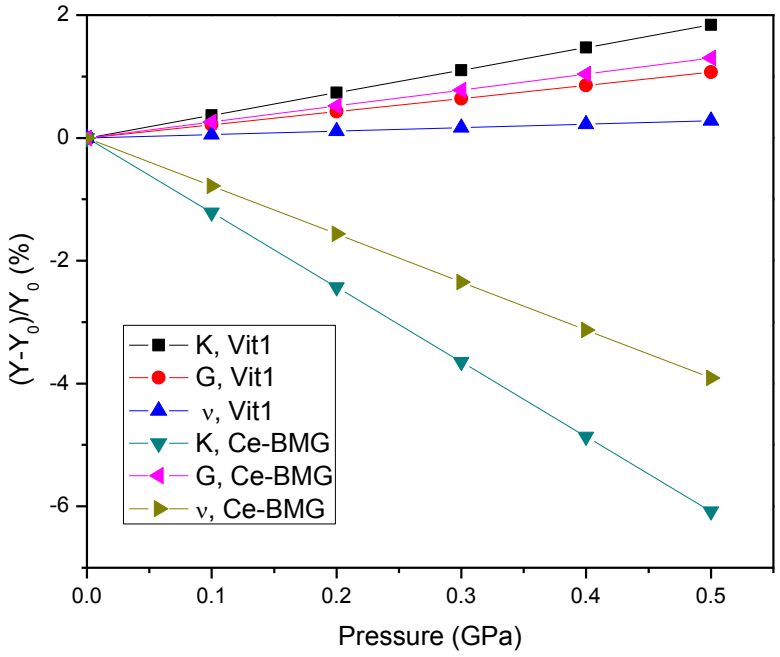

Fig. 1.6. Comparison of the relative variations of G, K and σ (ν) with pressure up to 0.5 GPa for the Ce-based BMG and Vit 1 at room temperature.[37]

1.4 Themes and Achievements

Metallic glass has been at the cutting edge of current metals research since it was discovered in 1960. As a newcomer in the glassy family, metallic glass opens new opportunities for both fundamental studies and commercial applications. Its unique random disordered and close-packed structure provides an ideal model system for studies of fundamental problems in condensed matter physics, such as glass structure, glass forming and supercooled liquid behavior. The polyamorphic phase transitions in traditional amorphous materials have improved our knowledge of amorphous matter. Generally, the polyamorphic phase transitions occur in open network glasses, but a series of pressure-induced transitions between two polyamorphs has been observed in Ce-based bulk metallic glasses in recent years. With the development of high pressure techniques, pressure is becoming an important variable just like of temperature or chemical composition for condensed phases. High pressure can cause a large change in atom spacing, chemical bonding and even the outer electron shells.

In this thesis, for the first time, the elastic sound wave velocities of $(La_{0.5}Ce_{0.5})_{64}Al_{16}Ni_5Cu_{15}$ bulk metallic glass are measured under high pressure up to 12 GPa using ultrasonic interferometry within a multi-anvil apparatus at room temperature. [40] Combined analysis of acoustic and P-V data allows a direct determination of the elastic moduli such as bulk modulus K, shear modulus G, Young's modulus E, and Poisson's ratio ν. The Debye temperature θ_D and Vickers hardness are also investigated to further understanding of its thermal and mechanical properties. All these results enable us to obtain insight into the high pressure behavior and physical properties of bulk metallic glass, and also further our understanding of the polyamorphism in Ce-based metallic glasses.

Chapter 2 Experimental Details

2.1 Synthesis and Characterization of La, Ce-based bulk metallic glasses

2.1.1 Synthesis

The sample was synthesized in collaboration with Q. S. Zeng et al. at the Laboratory of New-structured materials in Zhejiang University. Master ingots were prepared by arc-melting a mixture of pure lanthanum (99.5 atom%), cerium (99.5 atom%), aluminum (99.5 atom%), nickel (99.98 atom%), and copper (99.9 atom%) in a zirconium-gettered argon atmosphere. Each ingot was remelted five times to ensure compositional homogeneity. After polishing the surface mechanically, the ingot was heated in the crucible again then sucked into a copper mold for forming a rod. [41]

2.1.2 X-ray Diffraction

The structure of the sample was examined by X-ray diffraction (XRD) on a transverse section of a sample rod using a Thermo ARL X'Tra diffractometer with Cu K_α radiation at 45kV. The XRD pattern is shown in Fig. 2.1 (L32). The "hump" clearly indicates the amorphous structure of $(La_{0.5}Ce_{0.5})_{64}Al_{16}Ni_5Cu_{15}$ bulk metallic glass.

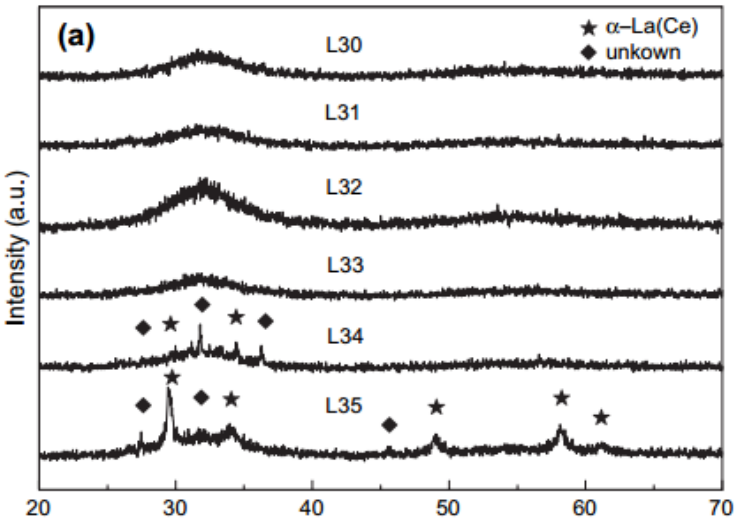

Fig. 2.1. XRD patterns for as-sucked $(La_{0.5}Ce_{0.5})_{60+x}Al_{20-x}Ni_5Cu_{15}$ (x=0, 2, 4, 6, 8 and 10 atom%) [41]

2.1.3 Bulk Density Measurement

Because the specimens are small and sometimes irregular in shape, the volume is difficult to obtain precisely using direct measurements. In this case, the bulk density of the specimen was measured using Archimedes' immersion method. The formula used is:

$$\rho_{sample} = \rho_{liquid} \times [\frac{W_{air}}{W_{air} - W_{liquid}}] \quad (2.1)$$

The sample weights in air (W_{air}) and liquid (W_{liquid}) were measured using a Mettler Balance, type AT261. The system was calibrated by determining the density of a single crystal MgO specimen having similar weight to that of each specimen and comparing the result with that for the MgO standard. The measured bulk density of the MgO single crystals are within 0.3% of the theoretical density. The liquid density (ρ_{liquid}) is determined at the measuring temperature and used to correct the sample density. For these measurements, carbon tetrachloride (CCl_4) was used as the immersion liquid. The bulk density of the sample at ambient conditions is 6.30(3) g/cm^3.

2.1.4 Acoustic Velocity Measurement at Ambient Conditions

A sample disk of 0.504 mm in length and 2.44mm in diameter was cut from the rod, and both faces of the sample were polished flat and parallel using 3μm and 1 μm diamond lapping films.

Ultrasonic travel times were measured for P and S waves in the ultrasonic laboratory at Stony Brook University. A parallel plated 40 MHz $LiNbO_3$ transducer (36° Y-cut for P waves and 41° X-cut for S waves) was mounted on one end of a glass buffer rod with Aremco Crystal-Bond allowing P and S wave travel times to be measured continuously between 20 MHz – 65 MHz and 20 MHz- 50 MHz, respectively. Fig. 2.2 is a schematic diagram showing the principle of travel time measurements.[42] A megahertz tone burst is transmitted via a piezoelectric transducer and buffer rod into the specimen. The propagating wave is partially reflected at the buffer-specimen interface (buffer rod echo) and the acoustic energy transmitted into the specimen is reflected from the far end of the specimen (specimen echo). These echoes then can be recorded and saved. A pulse-echo-overlap method [43] is used to obtain travel times. The velocities of the P and S waves of the specimen are calculated from the round trip travel times (t) and known sample length (L).

$$V=2L/t \tag{2.2}$$

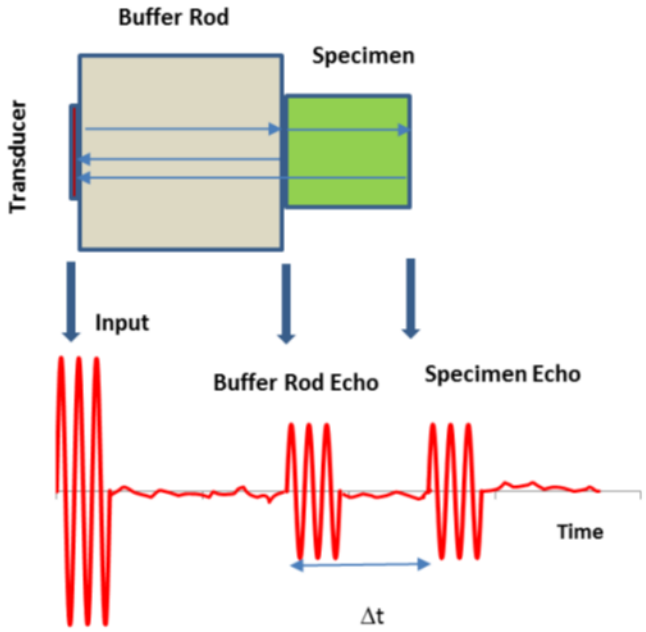

Fig.2.2. Schematic diagram for ultrasonic interferometric measurements. [42]

The ambient condition data provide a reference point for the determination of elastic properties as a function of pressure. Compressional and shear wave velocities are related to the elastic moduli by [44]

$$K = \rho(V_P)^2 - \frac{4}{3}\rho(V_S)^2 \tag{2.3}$$

$$G = \rho(V_S)^2 \tag{2.4}$$

$$E = \frac{9KG}{3K+G} \tag{2.5}$$

$$\nu = \frac{3K-2G}{2(3K+G)} \tag{2.6}$$

where K is the bulk modulus, G is the shear modulus, E is the Young's modulus and ν is Poisson's ratio. V_p and V_s are velocity of the compressional and shear waves, respectively. The

Debye temperature (θ_D) can also be derived from the acoustic velocities and density. Using acoustic data, θ_D at room temperature can be represented as [45]:

$$\theta_D = \frac{h}{k}\left(\frac{3nN_A}{4\pi}\right)^{1/3}\left(\frac{\rho}{\bar{M}}\right)^{1/3}\left(\frac{1}{3{V_P}^3} + \frac{2}{3{V_S}^3}\right)^{-1/3} \quad (2.7)$$

where h is Planck's constant, k is Boltzmann's constant, N_A is Avogadro's number, n is the number of atoms in the formula unit, ρ is the density and $\bar{M}$ is the mean atomic mass. All these values for the sample at ambient condition are shown in Table 2.1.

Table 2.1. Travel times, length, velocities, elastic moduli and the Debye temperature of $(La_{0.5}Ce_{0.5})_{64}Al_{16}Ni_5Cu_{15}$ bulk metallic glass at ambient conditions.

tp (μs)	**ts (μs)**	**Length (mm)**	**V_p (km/s)**	**V_s (km/s)**	**K (GPa)**	**G (GPa)**	**E (GPa)**	**ν**	**θ_D (K)**
0.3315(3)	0.6270(3)	0.504(1)	3.04(3)	1.61(2)	36.4(13)	16.3(4)	42.6	0.31	176.5

2.2 Ultrasonic Acoustic Velocity Measurements at High Pressure

2.2.1 High Pressure Apparatus

The 1000-ton uniaxial split cylinder apparatus (USCA-1000) at Stony Brook University was used for acoustic interferometry experiments at pressures up to around 12GPa. This apparatus consists of a 1000-ton Kennedy-Getting type hydraulic press (see Figure 2.3a) modified for use with a Walker-type split cylinder multi-anvil module (see Figure 2.3b). [46] The hydraulic press is the model #6kiloton Hydropress built in 1969 by the Advance Machine Corporation in Los Angeles, California, originally for use with piston and cylinder apparatus. More details of the apparatus are described in Li et al. [47] The Walker-type module is located on a horizontally traveling carriage and consists of six removable split sphere anvils inside a cylindrical containment ring with pressure distribution plates on both ends. A cubic cavity with a 50mm edge length is enclosed by these first stage anvils. Inside the cavity is the second stage anvil system of eight tungsten carbide cubes (MA-8). The cubes had 25.4 mm edge length and one corner truncated into a triangular surface with 8 mm edge length, thus creating an octahedral cavity in which the cell assembly was inserted. The cubes were separated by pyrophyllite gaskets and balsa wood spacers. The first stage anvils were insulated from the second stage by phenolic sheets glued to the cubes. A dual-mode $LiNbO_3$ transducer (10° Y-cut) was mounted outside one

cube for generating and receiving P and S wave signals simultaneously. The final assembled MgO octahedron and eight WC cubes are shown in Fig. 2.4.

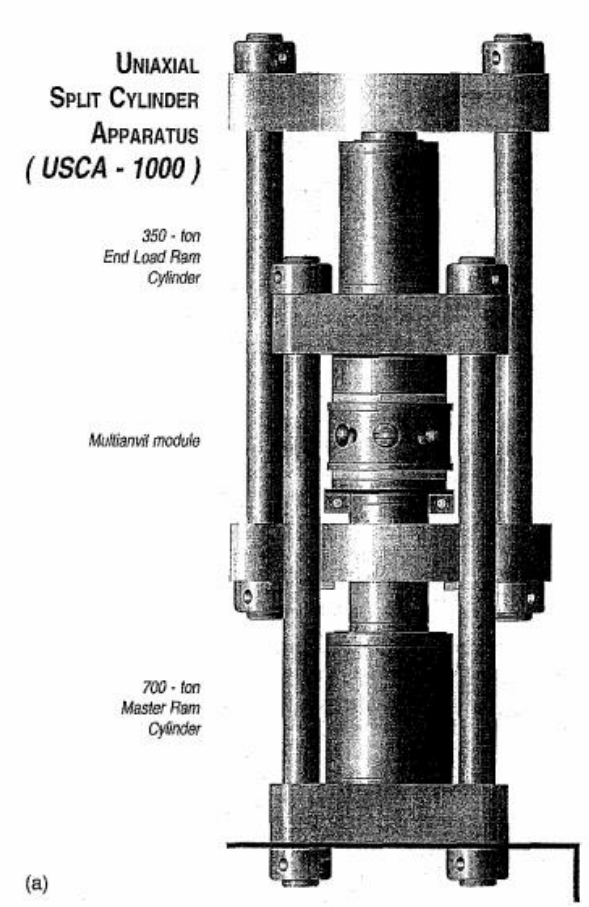

Fig. 2.3(a). The USCA-1000 high-pressure apparatus for acoustic wave experiments [47]

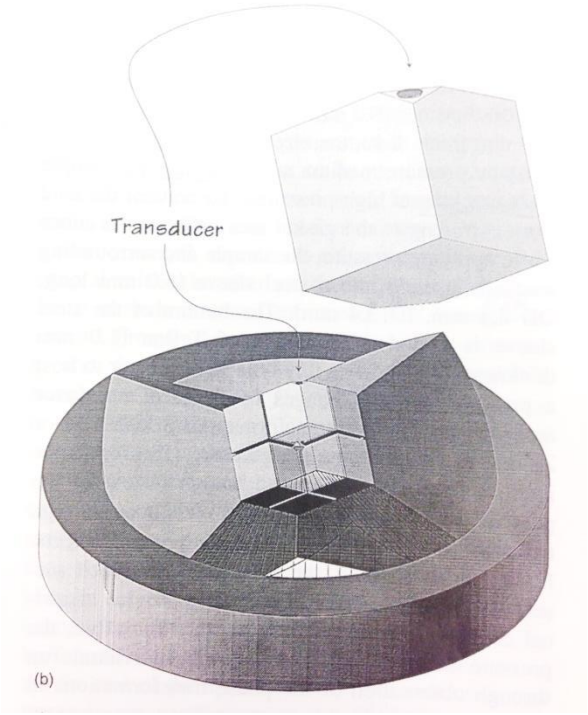

Fig. 2.3(b). Exploded view of the containment ring of the Walker module and the three removable split cylinders with the second stage WC cubes. The extracted view is of the cube used as a buffer rod, also showing the position of the ultrasonic transducer. [47]

Fig. 2.4. The final assembled MgO octahedron and eight WC cubes.

2.2.2 14/8 cell assembly

A cross-section of the pressure medium of the MgO octahedral cell assembly is shown in Fig. 2.5. An 8.3mm deep hole was drilled in one triangular face creating a cavity for the pressure medium and sample. On one end of the cell assembly, an alumina rod (~3.2mm in diameter, 3.8mm in length) served as an acoustic buffer rod and a pressure calibration. The sample was surrounded by a lead sleeve, thereby protecting the sample from cracking at high pressure and allowing the sample sit in the center of the cell tightly. On the other end, a disk of Teflon and a disk of Pb were inserted to provide a pseudo-hydrostatic pressure environment. A 2 μm thick gold foil was placed between the buffer rod and the sample as well as the buffer rod and WC cube to improve the mechanic coupling and to optimize the acoustic energy propagation into the sample.

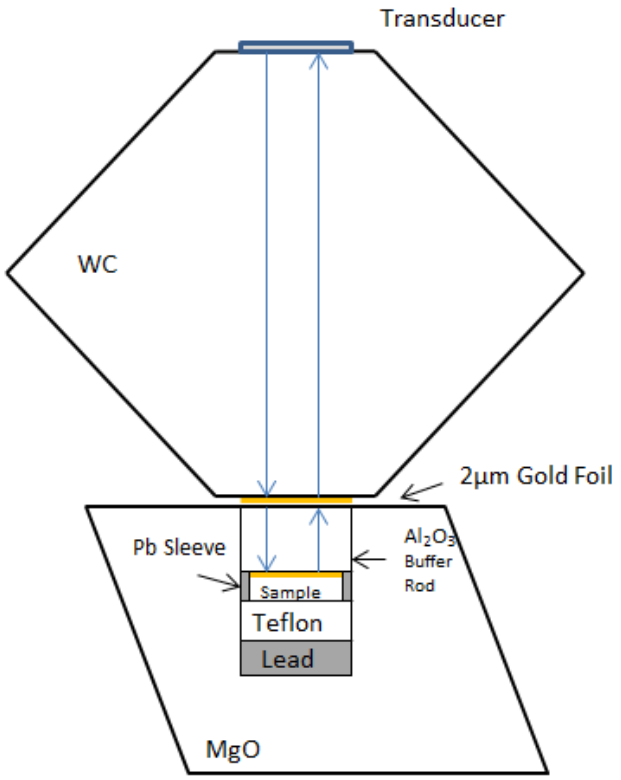

Fig. 2.5. A cross-section of the tungsten carbide (WC) cube and the MgO octahedral cell assembly.

2.2.3 Pressure Calibration

A detailed description of the pressure calibration technique for the USCA-1000 is given by Gasparik, [48] and Gwanmesia, Liebermann.[49] In this study, the cell pressure was calculated from the travel times of alumina buffer rod by equation [50]:

$$P = 1.50152 \times 10^4 \times (\frac{t_s}{t_0})^3 - 4.34801 \times 10^4 \times \left(\frac{t_s}{t_0}\right)^2 + 4.17157 \times 10^4 \times \left(\frac{t_s}{t_0}\right) - 1.32505 \times 10^4 \quad (2.5)$$

in which P is the pressure at the center of the cell assembly, t is the travel time of Al_2O_3 buffer rod and t_0 is the travel time at P=0. The observed variation of cell pressure with ram load is plotted in Fig. 2.6.

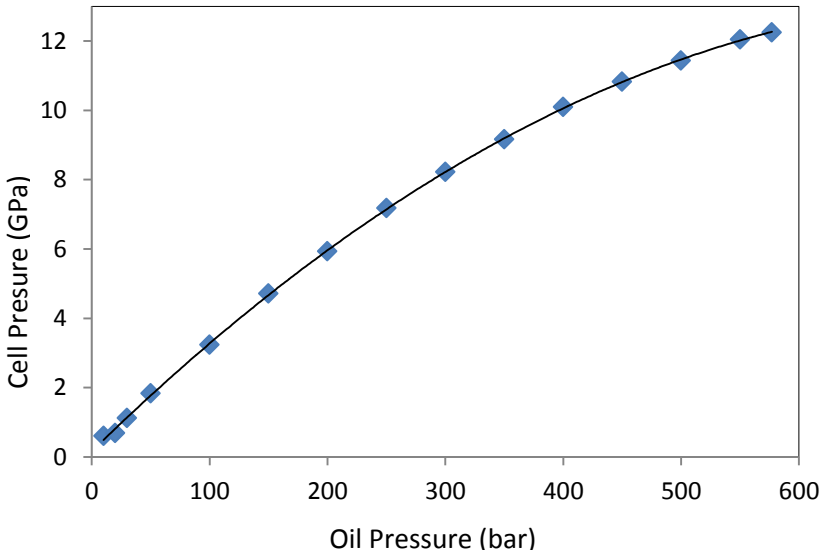

Fig. 2.6. The relationship between cell pressure and oil pressure obtained in acoustic velocity experiments

2.2.4 Travel Times Measurements

Travel times of P and S waves were measured as a function of pressure up to 12.2 GPa. For both P and S waves, acoustic waveform data were collected at intervals of 50 bar oil pressure while increasing the ram load, from which travel times were determined by using the interferometric method of pulse echo overlap (PEO) by overlapping buffer rod and sample echoes. Details about the transfer function method can be found elsewhere. [51] As an example,

real acoustic echoes observed for 50 MHz P wave at 9.6 GPa were shown in Fig. 2.7. The perturbation of the acoustic wave reverberation in the gold foil must be removed from the apparent travel times. The magnitude of the bond corrections is approximately 0.5 ns for P waves and 0.13 ns for S waves.

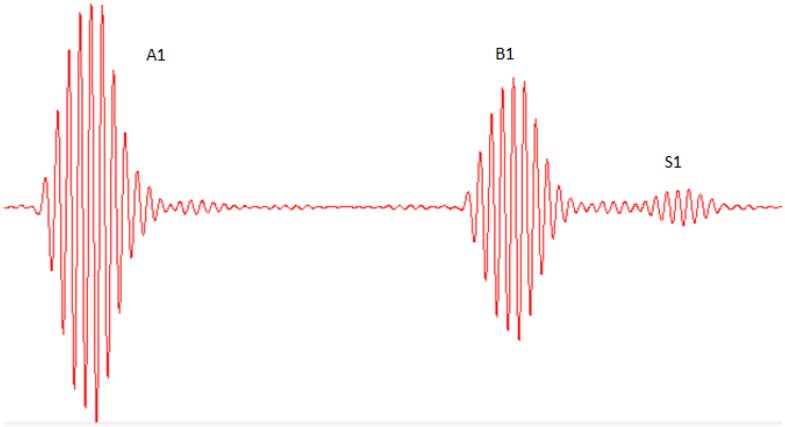

Fig. 2.7. Acoustic signals of P wave (50MHz) at 9.6 GPa. Three echoes are anvil echo (A1), the first buffer rod echo (B1) and the first specimen echo (S1), respectively.

Chapter 3 Results and Discussion

The results of ultrasonic measurements on $(La_{0.5}Ce_{0.5})_{64}Al_{16}Ni_5Cu_{15}$ bulk metallic glass under pressure up to 12.25 GPa are listed in Table 3.1 (a) and 3 (b), which represents pressurization and depressurization, respectively.

Table 3.1(a). Ultrasonic measurements data on pressurization

P (GPa)	**$2t_p$ (μs)**	**$2t_s$ (μs)**	**ρ (g/cm3)**	**L (mm)**	**V_p (km/s)**	**V_s (km/s)**
0.69	0.3495	0.6794	6.43(4)	0.501	2.86	1.47
1.12	0.3460	0.6754	6.51(4)	0.498	2.88	1.48
1.83	0.3460	0.6714	6.65(4)	0.495	2.86	1.47
3.23	0.3405	0.6704	6.91(4)	0.489	2.87	1.46
4.71	0.3315	0.6569	7.19(4)	0.482	2.91	1.47
5.93	0.3240	0.6464	7.41(4)	0.478	2.95	1.48
7.17	0.3095	0.6324	7.62(4)	0.473	3.06	1.50
8.22	0.2990	0.6219	7.79(4)	0.470	3.14	1.51
9.16	0.2890	0.6094	7.94(5)	0.467	3.23	1.53
10.10	0.2800	0.6014	8.08(5)	0.464	3.31	1.54
10.82	0.2730	0.5944	8.19(5)	0.462	3.38	1.55
11.44	0.2675	0.5874	8.28(5)	0.460	3.44	1.57
12.04	0.2645	0.5814	8.38(5)	0.458	3.47	1.58
12.25	0.2630	0.5789	8.41(5)	0.458	3.48	1.58

Table 3.1(b). Ultrasonic measurements data on depressurization

P (GPa)	$2t_p$ (μs)	$2t_s$ (μs)	ρ (g/cm^3)	L (mm)	V_p (km/s)	V_s (km/s)
12.14	0.2620	0.5784	8.39(5)	0.458	3.50	1.58
12.04	0.2625	0.5784	8.37(5)	0.459	3.49	1.59
11.83	0.2630	0.5764	8.33(5)	0.459	3.49	1.59
11.43	0.2650	0.5754	8.25(5)	0.461	3.48	1.60
11.32	0.2655	0.5759	8.23(5)	0.461	3.47	1.60
10.81	0.2675	0.5774	8.14(5)	0.463	3.46	1.60
10.29	0.2710	0.5794	8.05(5)	0.464	3.43	1.60
9.67	0.2745	0.5869	7.95(5)	0.466	3.40	1.59
9.04	0.2780	0.5899	7.85(5)	0.468	3.37	1.59
8.41	0.2815	0.5939	7.75(4)	0.470	3.34	1.58
7.26	0.2895	0.6009	7.58(4)	0.474	3.27	1.58
6.22	0.2970	0.6054	7.42(4)	0.477	3.21	1.58
4.89	0.3045	0.6144	7.21(4)	0.482	3.16	1.57
2.83	0.3130	0.6239	6.89(4)	0.489	3.13	1.57

Pressure induced changes in the sample dimensions were accounted for by using Cook's methods [52]:

$$\frac{L_0}{L} = 1 + \frac{1+\alpha\gamma T}{12\rho_0 {L_0}^2} \int \frac{1}{\frac{1}{(2t_p)^2} - \frac{4}{(3t_s)^2}} dP \qquad (3.1)$$

where ρ_o is the density, L_0 and L are sample length at ambient condition and high pressure, respectively, t_p and t_s are one way travel times of P and S waves through the sample, α is the thermal expansion coefficient and ν is the *Grüneisen* parameter. $(1+ \alpha\nu T) = C_p/C_v$ is the ratio of specific heats at constant pressure and volume, which is around 1.01 for most materials.[53] The elastic moduli and the Debye temperature on pressurization can be obtained by equations (2.3)-(2.7), which are listed in Table 3.2.

Table 3.2 The elastic moduli and the Debye temperature under pressure

P (GPa)	**K (GPa)**	**G (GPa)**	**ν**	**E (GPa)**	**Θ_D (K)**
0.69	34.1	14.0(5)	0.32	36.9	163.01
1.12	35.1	14.2(6)	0.32	37.5	164.02
1.83	35.2	14.5(6)	0.32	38.1	164.94
3.23	37.4	14.7(6)	0.33	39.0	165.33
4.71	40.2	15.5(6)	0.33	41.2	168.80
5.93	42.8	16.2(7)	0.33	43.1	171.61
7.17	48.5	17.1(7)	0.34	45.8	175.65
8.22	53.2	17.8(7)	0.35	48.0	178.79
9.16	58.0	18.6(8)	0.35	50.5	182.58
10.10	63.1	19.2(8)	0.36	52.3	185.18
10.82	67.4	19.8(9)	0.37	54.0	187.48
11.44	70.9	20.3(9)	0.37	55.7	189.79
12.04	72.9	20.8(9)	0.37	57.0	191.76
12.25	73.9	21.0(9)	0.37	57.1	192.60

On adiabatic compression, the third-order finite strain equations are expressed as the following [54]:

$$\rho {V_p}^2 = (1-2\varepsilon)^{\frac{5}{2}}(L_1 + L_2\varepsilon) \tag{3.2}$$

$$\rho {V_s}^2 = (1-2\varepsilon)^{\frac{5}{2}}(M_1 + M_2\varepsilon) \tag{3.3}$$

$$P = -(1-2\varepsilon)^{\frac{5}{2}}(C_1\varepsilon + \frac{C_2\varepsilon^2}{2}) \tag{3.4}$$

where the strain ε is given by

$$\varepsilon = \left[\left(1-\frac{\rho}{\rho_0}\right)^{\frac{2}{3}}\right]/2 \tag{3.5}$$

the coefficients are

$$C_1 = 3L_1 - 4M_1 \tag{3.6}$$

$$C_2 = 3L_2 - 4M_2 + 7C_1 \tag{3.7}$$

$$L_1 = K + \left(\frac{4}{3}\right) G \tag{3.8}$$

$$L_2 = 5\left(K + \frac{4G}{3}\right) - 3K(K' + \frac{4G'}{3}) \tag{3.9}$$

$$M_1 = G \tag{3.10}$$

$$M_2 = 5G - 3KG' \tag{3.11}$$

where K, G, K'and G' are the adiabatic elastic moduli and their pressure derivatives. Fitting all the present sound velocity data to the above equations, we obtained the bulk modulus (K), shear modulus (G) and their pressure derivatives at ambient conditions: for compression, K=30.0 (9) GPa ,G=12.6 (4) GPa, K'=2.70 and G'=0.78; for decompression, K=31.9 (9) GPa ,G=15.6 (4) GPa, K'=2.46 and G'=0.72 which show agreement with our results measured at room pressure and temperature (K=36.4 (13) GPa, G=16.3 (4) GPa). The slightly lower values derived from fitting to high pressure data are attributed to the inadequacy of 3rd order finite strain equation for describing the anomalous velocities in Fig. 3.1.

The acoustic velocities and density of the $(La_{0.5}Ce_{0.5})_{64}Al_{16}Ni_5Cu_{15}$ bulk metallic glass as a function of pressure are plotted in Fig. 3.1.

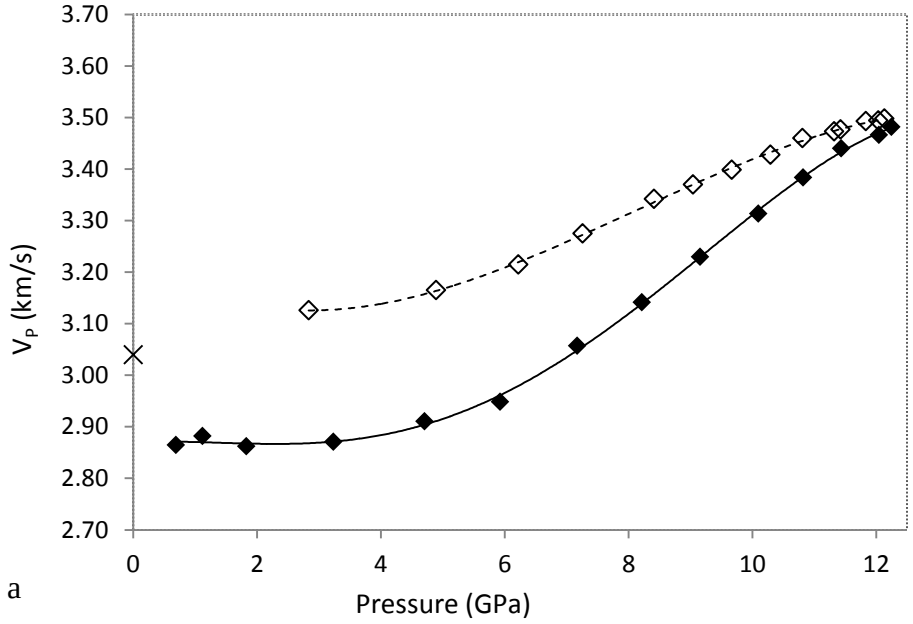
3.70
3.60
3.50
3.40
3.30
3.20
3.10
3.00
2.90
2.80
2.70
V_P (km/s)
0
2
4
6
8
10
12
Pressure (GPa)

a

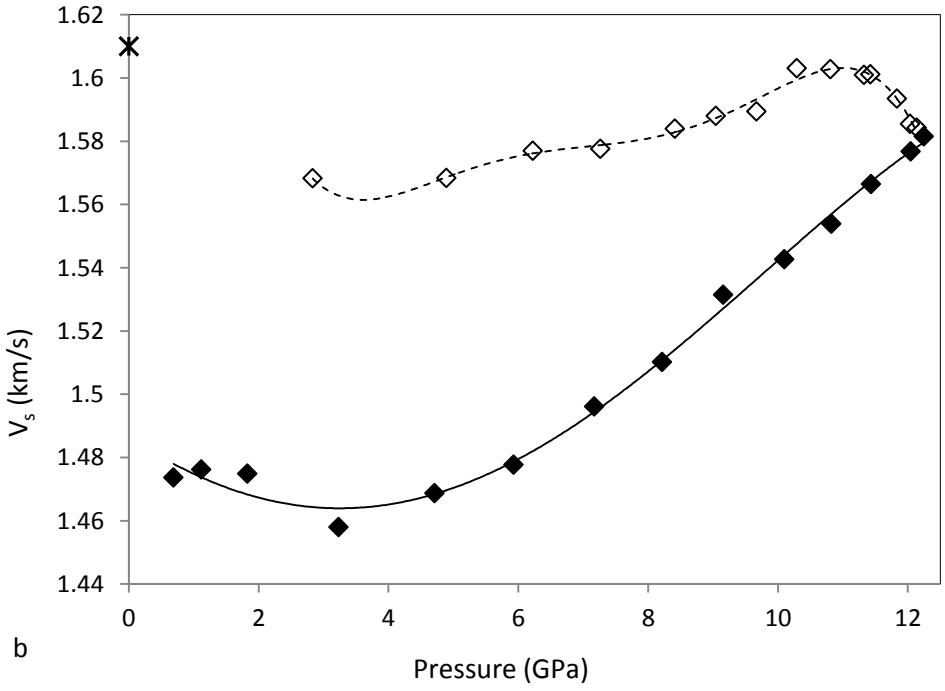
1.62
1.6
1.58
1.56
1.54
1.52
1.5
1.48
1.46
1.44
V_s (km/s)
0
2
4
6
8
10
12
Pressure (GPa)

b

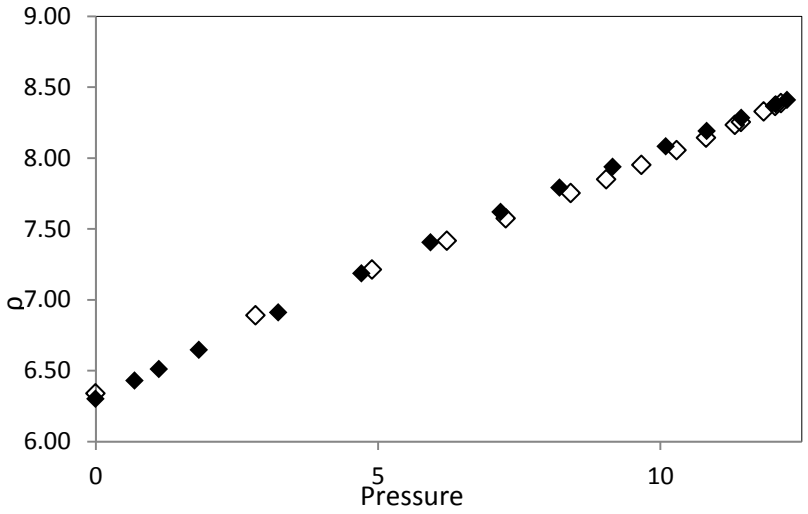

Fig. 3.1. Relative changes with pressure (a) V_p (b) V_s (c) ρ. Solid symbols are data on pressurization and open symbols are data on depressurization. The cross symbolizes the velocities of P and S waves at ambient conditions. Lines are polynomial fits as guides to the eye.

The density follows a nearly linear relation to pressure over the current pressure range (12.25 GPa), and almost identical with that on decompression. The density exhibits a much higher increase (up to 2.1%) than that of the other BMGs at 0.5 GPa and close to or even larger than that of the nonmetallic glasses such as oxides glasses as shown in Table 3.3. [36,55-56]

Table 3.3 The pressure-induced variations of ρ, V_p and V_s for various BMGs, oxide glasses and amorphous carbon. All the variations are at 0.5 GPa except for fused quartz at 0.43 GPa and window glass at 0.42 GPa. The data except for $(La_{0.5}Ce_{0.5})_{64}Al_{16}Ni_5Cu_{15}$ BMG are taken from Refs.[36,55-56]

Glasses	$\Delta\rho/\rho_0$ **(%)**	$\Delta V_p/V_{p0}$ **(%)**	$\Delta V_s/V_{s0}$ **(%)**
Fused quartz (0.43 Gpa)	1.24	-2.9	-2.49
Amorphous carbon	4.09	2.18	-3.09
Window glass (0.42 GPa)	1.08	-0.06	-1.19
SiO_2+TiO_2 glass	1.58	-4.57	-3.69
$Pd_{39}Ni_{10}Cu_{30}P_{21}$	0.32	0.75	0.51
$Zr_{41}Ti_{14}Cu_{12.5}Ni_{10}Be_{22.5}$	0.46	0.57	0.30
$Ce_{70}Al_{10}Ni_{10}Cu_{10}$	1.89	-2.66	-0.29
$(La_{0.5}Ce_{0.5})_{64}Al_{16}Ni_5Cu_{15}$	2.06	-5.92	-8.7

In this pressure region (up to 0.5 GPa), it is obvious that the changes of acoustic velocities as a function of pressure in these two Ce-based bulk metallic glasses are both negative, which is markedly different from other BMGs ,but rather similar to nonmetallic glasses. Fig. 3.2 compares the pressure variations of V_p and V_s, respectively, for bulk metallic glasses and nonmetallic glasses. As shown in Fig. 3.2, the pressure variation of V_p of La, Ce-based bulk metallic in this study is close to that of SiO_2+TiO_2 glass, but the pressure variation of V_s is larger than that of any glasses.

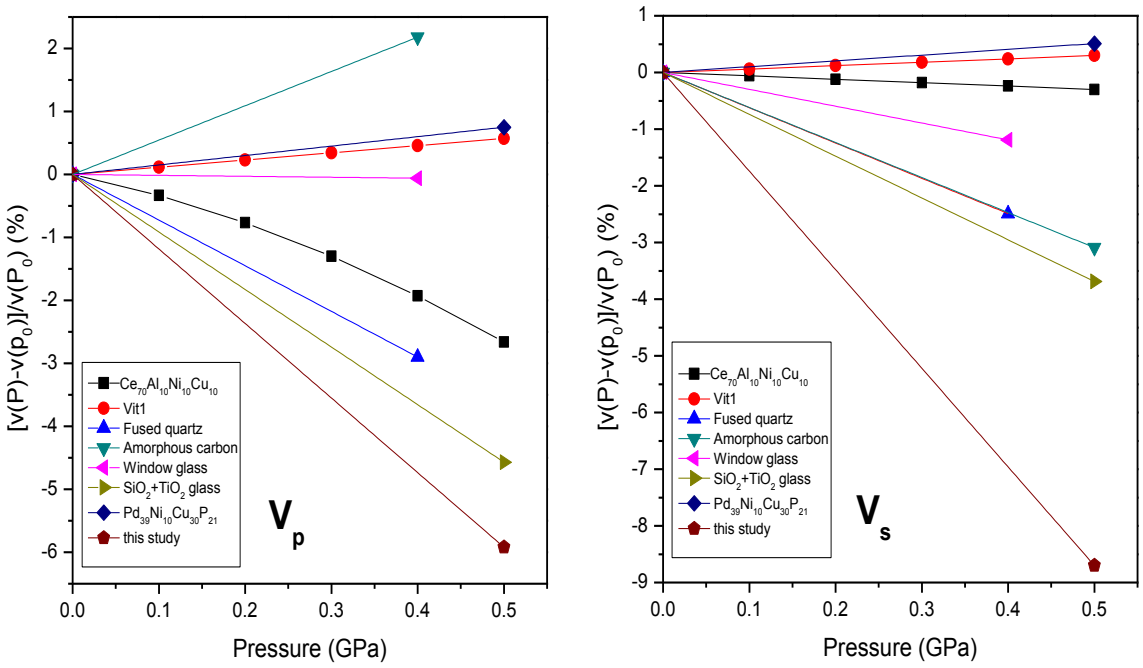

Fig. 3.2 A comparison of the acoustic velocities of V_p and V_s for BMG, $Pd_{39}Ni_{10}Cu_{30}P_{21}$ $Ce_{70}Al_{10}Ni_{10}Cu_{10}$, Vit1 ($Zr_{41}Ti_{14}Cu_{12.5}Ni_{10}Be_{22.5}$) and $(La_{0.5}Ce_{0.5})_{64}Al_{16}Ni_5Cu_{15}$, oxide glasses: fused quartz, window glass and SiO_2+TiO_2 glass, and amorphous carbon. [55]

For better understanding the mechanisms of such anomalous behavior, sound velocities as a function of pressure in SiO_2 glass measured by Brillouin scattering in diamond cells are shown in Fig. 3.3.[57] Minima were observed in both longitudinal and transverse velocities around 3 GPa and the results were in good agreement with those measured by ultrasonic techniques.[58] At pressures in excess of 3 GPa, the longitudinal and shear wave velocities increased rapidly corresponding to the pressure-induced coordination changes. [59] In our experiment, as shown in

Fig. 3.1(a) (b), sound velocities of La, Ce-based BMG also exhibit anomalous minima around 3 GPa and then increase gradually with pressure.

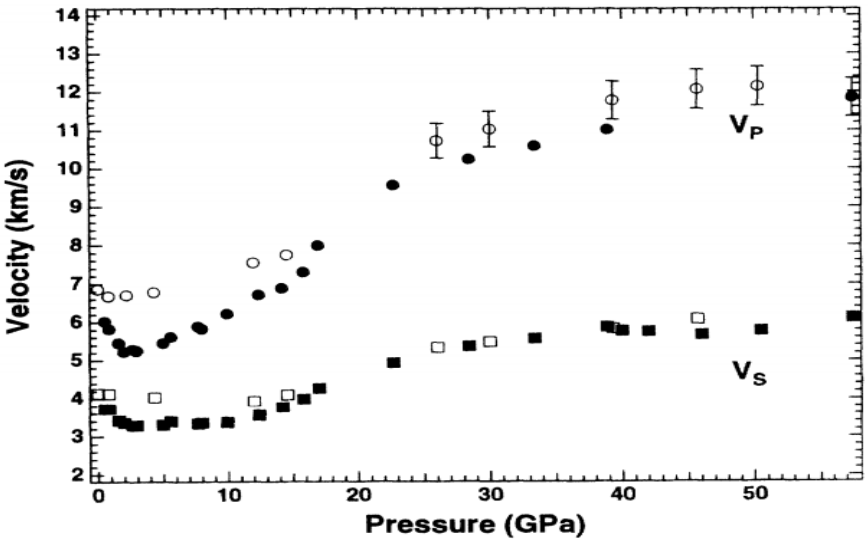

Fig. 3.3 Sound velocities in SiO_2 glass as a function of pressure. Solid symbols, compression; open symbols, decompression. [57]

These results above suggest that the Ce-based BMG may have certain structural similarities to that of silicate glasses. In a previous study, covalently-bonded structure mixing with metallic local bonding was proved to exist in Al-Ni-Ce melt-spin glasses.[60] Similar results were also found for $Ce_{70}Al_{10}Ni_{10}Cu_{10}$ BMG, which suggested that the covalently-bonded short-range ordering was the "rigid" structural units such as tetrahedral in oxide glasses and icosahedral cluster in some BMGs. [37] Combining these results with our experiment, it is reasonable to believe that complex bonding structures including metallic and covalent bonds coexist in the La, Ce-based BMG, and may be the cause of the anomalous acoustic behavior under pressure.

In recent years, polyamorphism, which was thought to occur only in glasses with directional and open structure, has been discovered in a series of Ce-based bulk metallic glasses under high pressure. A low density amorphous (LDA) to high density amorphous (HDA) transition was observed, and the large density difference was attributed to the special 4*f* -electron structure in Ce atoms. The transition pressure has a strong relation with the Ce content: that is 2-13.5 GPa for the $Ce_{55}Al_{45}$ metallic glass, and 1.5-5 GPa for the $Ce_{75}Al_{25}$ metallic glass. [38][61] It is natural to

raise the question: Does this polyamorphism happen in our La, Ce-based bulk metallic glass? Zeng et al. [39] have carried out an *in situ* high-pressure x-ray diffraction study on $(La_{0.5}Ce_{0.5})_{64}Al_{16}Ni_5Cu_{15}$ bulk metallic glass. Samples were compressed up to 40 GPa using a Mao-Bell-type diamond-anvil cell and diffraction patterns were recorded by a CCD detector. Bulk modulus as a function of pressure was plotted according to the parameter $[d\,max(P)/d\,max(0)]^3$, which is proportional to the reduced volume of the sample, changes with pressure. A discontinuity in the bulk modulus at about 14 GPa was detected as shown in Fig. 3.4. This sudden change in compressibility was attributed to the Kondo coupling between 4*f* spin and conductive electrons. The bulk modulus as a function of pressure obtained in our experiment was also shown in Fig. 3.4. By a linear fitting to the data, the pressure derivative of the bulk moduli changed at around 5.9 GPa, which was not found in Zeng's study. The difference in the bulk moduli at low pressure range may be caused by the two different methods of measurement.

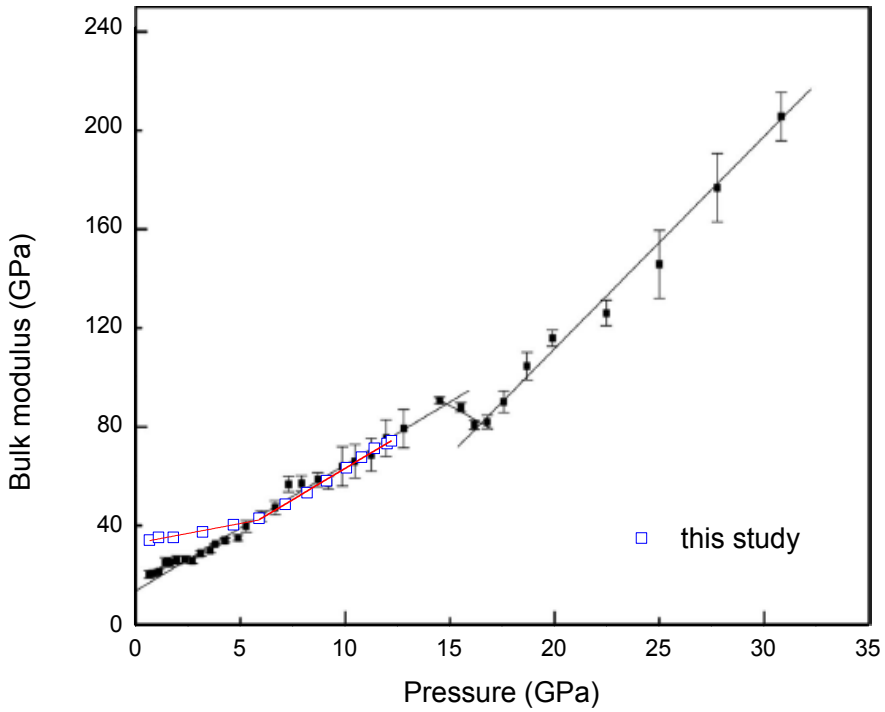

Fig. 3.4. Bulk modulus K vs. pressure for $(La_{0.5}Ce_{0.5})_{64}Al_{16}Ni_5Cu_{15}$ bulk metallic glass. The blue markers are data from this study. Red straight lines are linear fittings. The black ones are data from Zeng's study. [39]

As examination of the pressure dependence of both bulk and shear moduli, showing in Fig. 3.5, there are abrupt increases in both the bulk and shear moduli at about 5.9 GPa. Below 5.9

GPa, the derivatives are $\frac{\partial G}{\partial P} = 0.39(3)$, $\frac{\partial K}{\partial P} = 1.60(12)$. Above 5.9 GPa, the derivatives are $\frac{\partial G}{\partial P} = 0.769(1)$, $\frac{\partial K}{\partial P} = 5.04(9)$. These discontinuities in the slope of the elastic moduli, also consistent with the sound wave velocities changes displayed in Fig. 3.1, are suggestive of a structural change indeed occurring in $(La_{0.5}Ce_{0.5})_{64}Al_{16}Ni_5Cu_{15}$ bulk metallic glass.

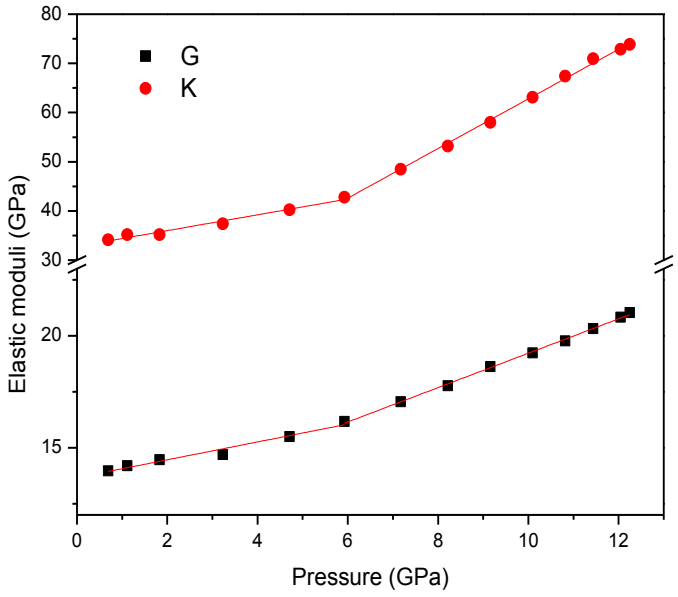

Fig. 3.5. Bulk (K) and shear (G) moduli of the $(La_{0.5}Ce_{0.5})_{64}Al_{16}Ni_5Cu_{15}$ BMG as a function of pressure. Lines are linear fitting to the data above and below 5.9 GPa.

The equation of state (EOS) relating volume and pressure plays an important role in understanding the microstructure and phase transition of compressed solids under high pressure. In our experiment, the sample was considered to be compressed elastically under hydrostatic pressure, thus $\frac{V}{V_0} = (\frac{L}{L_0})^3$, where V_0 is 28.0 Å^3 per atom and L_0 is 0.504 mm. The density of the glass at zero pressure (P_0) determined using Archimedes' method, is 6.30 g /cm^3. The pressure-volume (P-V) equation of state (EOS) of La, Ce-based BMG from this study is plotted in Fig. 3.6 for comparison with amorphous $Ce_{55}Al_{45}$. [38] The magenta and blue diamond symbols are data from compression and decompression in this study. It is interesting to notice that the compressibility of the La, Ce-based BMG is almost identical to that of $Ce_{55}Al_{45}$ amorphous glass, but our result shows that there is no hysteresis loop in a compression-decompression cycle over the current pressure range (12.25 GPa). This reversible pressure dependence of the volume is also reported in the $La_{75}Al_{25}$ metallic glass. [38] Although Lanthanum is the first element in the

lanthanides, Cerium is the first one with 4f electron structure which is responsible for special properties. It is believed that 4f electronic delocalization causes the $\alpha \Leftrightarrow \gamma$ transition in crystalline Ce.[62] For $Ce_{55}Al_{45}$ BMG, Sheng et al. have presented a structural model in which a double shell feature in the Ce-Ce neighbor was observed at the transition using the inverse Monte Carlo (IMC) simulation method. At the transition, one of the Ce-Ce shells had a much shortened bond length attributed to closer Ce-Ce interactions and *f* electron delocalization, which enhanced the electronic bonding.[38] Belhadi et al. also provided experimental evidence for this structural rearrangement in Ce-Ce shell environment in $Ce_{60}Al_{20}Cu_{20}$ BMG using x-ray absorption techniques. [63] They noticed that the average Ce-Ce bond compressed while the Ce-Al and the Ce-Cu shells expanded or remained unchanged. In our experiment, the synthesis of $(La_{0.5}Ce_{0.5})_{64}Al_{16}Ni_5Cu_{15}$ BMG [41] suggested this BMG was obtain by adjusting the contents of Al and Cu based on $(La_{0.5}Ce_{0.5})_{60}Al_{20}Cu_{20}$ BMG which may have similar local structure with $Ce_{60}Al_{20}Cu_{20}$ BMG. Thus, it is reasonable to believe that the polyamorphism happen because of the Ce-Ce bond existing in La, Ce-based BMG, but the reason why there is no hysteresis loop as shown in Fig. 3.6 remains unclear. One possibility is that the pressure range of the current study is within the reported transition region. In this study, the content of Ce is 32 at.% which is less than that in binary or ternary Ce-based BMGs involving 4*f* electron delocalization. The addition of Lanthanum may also influence the Ce-Ce shell environment. More investigation is still needed to understand the origin and mechanisms of polyamorphism in La, Ce-based BMG.

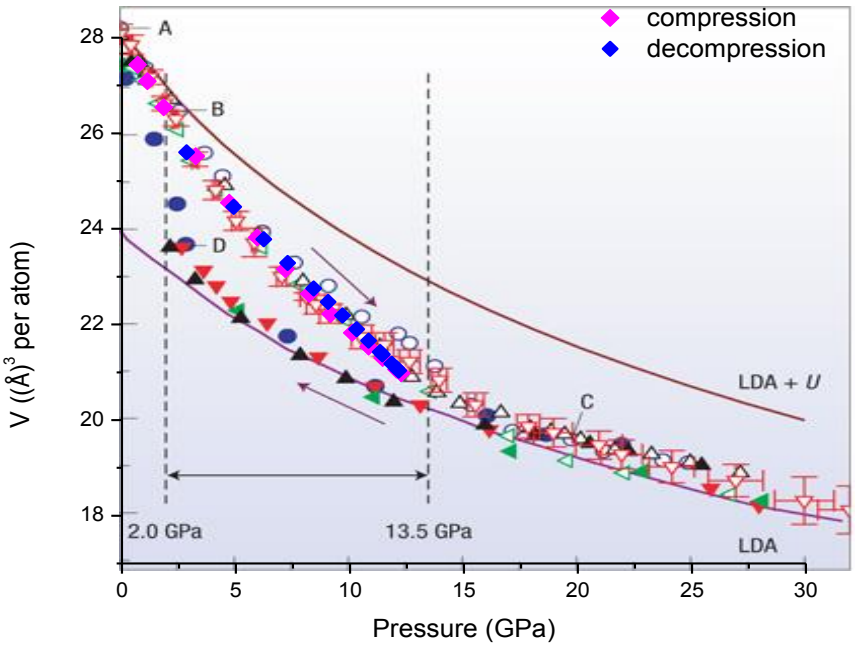

Fig. 3.6. A comparison of the P-V EOS for $(La_{0.5}Ce_{0.5})_{64}Al_{16}Ni_5Cu_{15}$ BMG and amorphous $Ce_{55}Al_{45}$. [38] The diamond symbols in magenta and blue are data in this study.

The Debye temperature θ_D of the BMGs can be derived from the acoustic velocities and density by equation 2.7. It is interesting to seek a possible connection between the Debye temperature θ_D and the glass transition temperature T_g. Modifying to the Lindemann melting criterion[64], Wang et al. described this correlation in the following form [65]:

$$T_g = aM{\theta_D}^2 \tag{3.12}$$

where a is a constant with values for BMGs ranging from 1.0×10^{-4} to 1.4×10^{-4} $(K\ mol)^{-1}$, M is the average atomic mass and θ_D is the Debye temperature. Using the obtained acoustic velocities and density at ambient conditions (V_p=3.04(3) km/s, V_s=1.61(2) km/s, ρ=6.30(3) g/cm^3), the Debye temperature for $(La_{0.5}Ce_{0.5})_{64}Al_{16}Ni_5Cu_{15}$ BMG is 176.5 K and the glass transition temperature is 396.5 K (when a=1.2×10^{-4} $(K\ mol)^{-1}$), which is in good agreement with the value 403 K reported by Zeng et al. [41]

As a potential functional material, the Vickers hardness H_v is one of the important physical properties in bulk metallic glasses. The intrinsic correlation between hardness and elastic moduli also attracts much attention. Wang et al. [34] reported the correlation between hardness H_v and

Young's modulus as: $E/H_v \approx 20$ and Chen et al. [66] also suggested the Vickers hardness linearly correlating with the shear modulus ($H_v = 0.151G$). According to Wang's and Chen's relations, the Vickers hardness in this study was determined to be 2.1 GPa and 2.5 GPa, respectively, and the former yields a value closer to the experimental hardness 1.9 GPa.[41]

In composite materials, the rule of mixtures can be used to predict the elastic modulus of a composite from the elastic moduli and volume fractions. Voigt and Reuss developed the upper and lower bound of the rule of mixtures by assuming either strain continuity or stress continuity, respectively. [67,68] To average the Voigt and Reuss bounds, the Voigt-Reuss-Hill (VRH) approximation was obtained and has been widely used to calculate the elastic moduli of isotropic polycrystalline materials and mineral aggregates.[69] The Reuss, Viogt and Hill approximations (M_R, M_V and M_{VRH}) are described as:

$$M_R = \left[\sum_{i=1}^{N} f_i {M_i}^{-1}\right]^{-1} \tag{3.13}$$

$$M_V = \sum_{i=1}^{N} f_i M_i \tag{3.14}$$

$$M_H = (M_R + M_V)/2 \tag{3.15}$$

where M is the elastic moduli K and G, f_i is the atomic percentage of element i.

For metallic glasses, the VRH approximation was found to successfully predict the elastic moduli of some BMG systems, even though the atomic structure of BMG is believed to be different from a simple compaction of elemental metals. [53, 70, 71] As an exercise, the elastic moduli of the La, Ce-based BMG were also estimated by the VRH approximation from its constituent metals and the results are listed in Table 3.4.

Table 3.4. Elastic moduli of La, Ce-based BMG and constituent metals at ambient conditions. Data of metals are from the website. (http://www.webelements.com)

sample	ρ (g/cm^3)	G (GPa)		K (GPa)	
$(La_{0.5}Ce_{0.5})_{64}Al_{16}Ni_5Cu_{15}$	6.3	G_R=15.6 G_V=18.5 G_H=17.1	$G_{exp.}$=16.3(4)	K_R=28.5 K_V=40.2 K_H=34.4	$K_{exp.}$=36.4(13)
La	6.15	14		28	
Ce	7.14	14		22	
Al	2.7	26		76	
Ni	8.902	76		180	
Cu	8.954	48		140	

It is interesting to notice that the results are in agreement with those obtained by ultrasonic method in this study. Equation 3.13 (the Reuss bound G_R=15.6 GPa) gives an upper bound, while equation3.14 (the Voigt bound G_V=18.5 GPa) gives a lower bound and their average value given by Hill (G_H=17.1GPa) shows a close estimation of the elastic moduli of BMGs at ambient conditions. This result indicates again that the elastic moduli of the BMGs may strongly depend on the properties of the constituent elements that are intrinsic to their crystalline form, such that the BMGs can be closely modeled as highly dense packing structure. [72, 73] More investigations are still needed in understanding the intrinsic microstructure of metallic glasses and the nature of glasses.

Chapter 4 Conclusion

In this study, P and S sound wave velocities of the $(La_{0.5}Ce_{0.5})_{64}Al_{16}Ni_5Cu_{15}$ bulk metallic glass are measured successfully under high pressure up to 12.3 GPa using ultrasonic interferometry in a multi-anvil apparatus. The elastic moduli, bulk modulus K and shear modulus G and their pressure derivatives are calculated using third-order Eulerian finite strain equations: for compression, K=30.0 (9) GPa, G=12.6 (4) GPa, K'=2.70 and G'=0.78; for decompression, K=31.9 (9) GPa, G=15.6 (4) GPa, K'=2.46 and G'=0.72. Both P and S waves exhibit softening behavior at low pressure that is consistent with previous study. It implies that the Ce-based bulk metallic glass contains short-range covalent like bonds similar to those of silicate glasses. No permanent densification was observed. I also find that slopes of elastic moduli as a function of pressure change at around 5.9 GPa. Compared with other studies on Ce-based BMG, it is reasonable to believe that a second order polyamorphic phase transition occurs in $(La_{0.5}Ce_{0.5})_{64}Al_{16}Ni_5Cu_{15}$ bulk metallic glass. The good agreement in density between those along compression and decompression suggests the transition is reversible.

Other important elastic moduli are also calculated from the acoustic velocities, including the Young's modulus E=42.6 GPa and the Poisson's ratio ν=0.31 at ambient conditions. The calculated Debye temperature and Vickers hardness are obtained which show good agreement with previous experimental results. Our study provides a direct method to obtain the elastic properties of Ce-based BMG under high pressure and indeed can provide insight on microstructural characteristics and bonding nature of the bulk metallic glass.

In the future work, loading and unloading cycles should be carried out on the same specimen to investigate whether this transition is reversible and provide more information on understanding the anomalous acoustic behaviors. Ultrasonic measurements at pressure can be performed using a DIA-type, large-volume apparatus (SAM85) in conjunction with *in situ* x-ray techniques in order to obtain the exact sample length and its amorphous peak change simultaneously. [74]

Reference

1. http://en.wikipedia.org/wiki/Amorphous_solid

2. W. Klement, R. H. Willens, P. Duwez, *Non- crystalline structure in solidified gold-silicon alloys*. Nature 187 (1960) 869-70

3. H.S. Chen, D. Turnbull. *Stability and structure of palladium-silicon based alloy glasses*. Acta Metall, 17 (1969) 1021

4. H.S. Chen, *Thermodynamic considerations on the formation and stability of metallic glasses*. Acta Metall, 22 (1974) 1505

5. Mark C. Lee, James M. Kendall, William L. Johnson, *Spheres of the metallic glass $Au_{55}Pb_{22.5}Sb_{22.5}$ and their surface characteristics*. Appl. Phys. Lett. 40, 382 (1982)

6. A. J. Drehman, A. L. Greer, D. Turnbull, *Bulk formation of a metallic glass: $Pd_{40}Ni_{40}P_{20}$* . Appl. Phys. Lett. 41, 716 (1982)

7. H. W. Kui, A. L. Greer, D. Turnbull, *Formation of bulk metallic glass by fluxing*. Appl. Phys. Lett. 45, 615 (1984)

8. A. Inoue, T. Zhang, T. Masumoto, *Al-La-Ni amorphous alloys with a wide supercooled liquid region*. Mater. Trans. JIM 30 (1989) 965-72

9. A. Inoue, T. Nakamura, T. Sugita, T. Zhang, T. Masumoto, *Bulky La-Al-TM (TM=Transition Metal) Amorphous Alloys with High Tensile Strength Produced by a High-Pressure Die Casting Method*. Mater. Trans. JIM 34 (1993) 351

10. A. Inoue, A. Kato, T. Zhang, S. G. Kim, T.Masumoto. *Mg-Cu-Y Amorphous Alloys with High Mechanical Strengths Produced by a Metallic Mold Casting Method*. Mater Trans JIM 1991;32:609-616

11. T. Zhang, A. Inoue, T. Masumoto. *Amorphous Zr–Al–Tm (Tm=Co, Ni, Cu) alloys with significant supercooled liquid region of over 100 K*. Mater Trans JIM, 32 (1991) 1005–1010

12. A. Peker, and W.L. Johnson,, Patent, U.S. No. 5,288,344 (1994)

13. A. Peker, PhD dissertation, California Institute of Technology, 1994

14. X.H. Lin, W.L. Johnson, *Formation of Ti–Zr–Cu–Ni bulk metallic glasses.* J. Appl. Phys. 78 (1995) 6514

15. A. Peker, W. L. Johnson, *A highly processable metallic glass: $Zr_{41.2}Ti_{13.8}Cu_{12.5}Ni_{10.0}Be_{22.5}$*. Appl. Phys. Lett. 63, 2342 (1993)

16. W.L. Johnson, *Bulk Glass-Forming Metallic Alloy: Science and Technology*, MRS Bull. 24 (10) (1999) 42

17. A. Inoue, N. Nishiyama, H. Kimura, *Preparation and thermal stability of bulk amorphous $Pd_{40}Cu_{30}Ni_{10}P_{20}$ alloy cylinder of 72 mm in diameter*. Mater Trans JIM, 38 (1997) 179–183

18. N. Nishiyama, K. Takenaka, H.Miura, N. Saidoh, Y. Zeng, A. Inoue, *The world's biggest glassy alloy ever made*. Inermatellics 30 (2014) 19-24

19. Jörg F. Löffler, *Bulk Metallic Glasses*. Intermetallics, 11(6), 2003

20. W. H. Wang, *Bulk metallic glasses with functional physical properties*. Adv. Mater. 21 (2009) 4524-4544

21. A. Inoue, A. Takeuchi, *Recent development and application products of bulk glassy alloys*. Acta Materialia, 59 (6), 2011, 2243-2267

22. J. D. Bernal, *Geometry of the structure of monatomic liquids*. Nature 185 (1960) 68–70

23. P. H. Gaskell, *A new structural model for transition metal-metalloid glasses*. Nature 276 (1978) 484–85

24. P. H. Gaskell, *A new structural model for amorphous transition metal silicides, borides, phosphides and carbides*. J. Non-Cryst. Solids 32 (1979) 207–24

25. A. Inoue, T. Negishi, H.M. Kimura, T. Zhang, A. R. Yavari *High packing density of Zr- and Pd-based bulk amorphous alloys*. Mater. Trans. JIM 39 (1998) 318–21

26. W. K. Luo, H. W. Sheng, F. M. Alamgir, J. M. Bai, J. H. He, E. Ma, *Icosahedral short-range order in amorphous alloys*. Phys. Rev. Lett. 92 (2004) 145502

27. M. W. Chen, A. Inoue, T. Zhang, A. Sakai, T. Sakurai, *Formation of icosahedral quasicrystals in an annealed $Zr_{65}Al_{7.5}Ni_{10}Cu_{12.5}Ag_5$ metallic glass*. Philos. Mag. Lett. 80 (2000) 263–69

28. D. B. Miracle, *The efficient cluster packing model: an atomic structural model for metallic glasses*. Acta Mater. 54 (2006) 4317–36

29. D. B. Miracle, *A structural model for metallic glasses*. Nat. Mater. 3 (2004) 697–702

30. H. W. Sheng, W. K. Luo, F. M. Alamgir, J. M. Bai, E. Ma, *Atomic packing and short-to-medium-range order in metallic glasses*. Nature 439 (2006) 419–25

31. J. Xu, M. H. Manghnani, *Brillouin-scattering studies of a sodium silicate glass in solid and melt conditions at temperatures up to 1000 °C.* Phy. Rev. B 45 (1992) 640

32. P.W. Bridgman, *Pressure-Volume Relations for Seventeen Elements to 100,000 kg/cm^3*. Proc. Am. Acad. Arts Sci. 74(1941) 425

33. W. H. Wang, H. Y. Bai, J.L Luo, R. J. Wang and D. Jin, *Supersoftening of transverse phonons in $Zr_{41}Ti_{14}Cu_{12.5}Ni_{10}Be_{22.5}$ bulk metallic glass*. Phys. Rev. B 62, 25, 2000

34. W. H. Wang, *The elastic properties, elastic models and elastic perspectives of metallic glasses.* Progress in Materials Science 57 (2012) 487

35. W. H. Wang, F.Y Li, M.X Pan, D.Q Zhao, Ru Ju Wang, *Elastic property and its response to pressure in a typical bulk metallic glass*, Acta Mater 2004. 52,715

36. R. J. Wang, F. Y. Li, J. F. Wang and W. H. Wang, *Responses of glassy structure and properties to pressure and devitrification*, Appl. Phys. Lett. 83, 2814 (2003)

37. B. Zhang, R.J. Wang, W.H. Wang, *Unusual responses of acoustic and elastic properties to pressure and crystallization of Ce-based bulk metallic glass*, Phys. Rev. B, 72 (2005) 104205

38. H.W. Sheng, H.Z. Liu, Y.Q. Cheng, J. Wen, P.L. Lee, W.K. Luo et al. *Polyamorphsim in metallic glasses*, Nat. Mater, 6 (2007) 192

39. Q.S. Zeng, Y.C. Li, C.M. Feng, P. Liermann, M. Somayazulu, G.Y. Shen et al. *Anomalous compression behavior in lanthanum/cerium-based metallic glass under high pressure*. Proc Natl Acad Sci USA, 104 (2007) 13565

40. B. Li, I. Jackson, T. Gasparik, R. C. Liebermann, *Sound velocities of olivine and beta polymorphs of Mg2SiO4 at Earth's transition zone pressures*. Physics of the Earth and Planetary Interiors, 98 (1996) 79

41. Q.S. Zeng, J.F. Liu, G.Q. Zhang, L.N. Wang, J.Z. Jiang, *Synthesis of LaCe-based bulk metallic glasses with low glass transition temperature*, Intermetallics, 15 (2007) 753

42. B. Li, R. C. Liebermann, *Study of the Earth's Interior using measurements of sound velocities in minerals by ultrasonic interferometry*, in press.

43. E. P. Papadakis, *Ultrasonic phase velocity by the pulse-echo overlap method incorporating diffraction phase corrections.* J. Acoust. Soc. Am. 42 (1967) 1045

44. D. Schreiber, *Elastic constants and their measurement*. McGraw-Hill, New York (1973), pp. 35–81 (chapter 3)

45. C. Kittel, *Introduction to solid state physics(6th ed.).* John Wiley & Sons Inc., New York (1986)

46. D. Walker, M. A. Carpenter, C. M. Hitch, *Some simplifications to multi-anvil devices for high pressure experiments*. Am. Mineral., 75 (1990) 1020

47. B. Li, I. Jackson, T. Gasparik, R. C. Liebermann, *Elastic wave velocity measurement in multi-anvil apparatus to 10 GPa using ultrasonic interferometry*. Phys. Earth Planet. Inter. 98 (1996) 79-91

48. T. Gasparik, *Phase relations in the transition zone*. J. Geophys. Res. 95 (1990) 15751

49. G. D. Gwanmesia, R. C. Liebermann, *Polycrystals of high-pressure phases of mantle minerals: Hot pressing and characterization of physical properties, High-pressure Research: Application to Earth and Planetary Sciences, edited by Y. Syono and M. Manghnani*, American Geophysical Union, Washington, D. C., (1992) 117-135

50. Wang et al. in preparation

51. B. Li, K. Chen, J. Kung, R. C. Liebermann, D. J. Weidner, *Sound velocity measurement using transfer function method*. J. phys. –Condens. Mat. 14 (2002) 11337

52. R. K. Cook, *Variation of elastic constants and static strains with hydrostatic pressure: A method for calculation from ultrasonic measurements*. J. Acoust. Soc. Am. 29 (1957) 445

53. W. Liu, Q. S. Zeng, Q. K. Jiang, L. P. Wang, B. S. Li, Density and elasticity of $Zr_{46}Cu_{37.6}Ag_{8.4}Al_8$ bulk metallic glass at high pressure. Sripta Materialia 65 (2011) 497

54. G. F. Davies, A. M. Dziewonski, *Homogeneity and constitution of the Earth's lower mantle and outer core*. Phys. Earth Planet. Inter. 10 (1975) 336

55. W. H. Wang, R. J. Wang, F. Y. Li, D. Q. Zhao, M. X. Pan, *Elastic constants and their pressure dependence of* $Zr_{41}Ti_{14}Cu_{12.5}Ni_9Be_{22.5}C_1$ *bulk metallic glass.* Appl. Phys. Lett. 74 (1999) 1803

56. L. M. Wang, L. L. Sun, W. H. Wang, R. J. Wang, W. K. Wang, *Elastic constants of Pd39Ni10Cu30P21 bulk metallic glass under high pressure*. Appl. Phys. Lett. 77 (2000) 3734

57. C. Zha, R. J. Hemley, H. Mao, T. S. Duffy, C. Meade, *Acoustic velocities and refractive index of SiO2 glass to 57.5 GPa by Brillouin scatterin*g, Phys. Rev. B 50 (1994)

58. K. Kondo, S. Ito, A. Sawaoka, *Nonlinear pressure dependence of the elastic moduli of fused quartz up to 3 GPa*. J. Appl. Phys. 52 (1981) 2826

59. T. Sasakura, K. Suito, H. Fujisawa, in High Pressure Science and Technology, edited by N. V. Novikov and Y. M. Chistyakov (Naukova Dumka, Kiev, 1989), p. 60.

60. A. N. Mansour, C.-P. Wong, R. A. Brizzolara *Atomic structure of amorphous* $Al_{100-2x}Co_xCe_x$ *(x=8, 9, and 10) and* $Al_{80}Fe_{10}Ce_{10}$ *alloys: An XAFS study*. Phys. Rev. B 50 (1994) 12401

61. Q. Zeng, Y. Ding, W. L. Mao, W. Yang, S. V. Sinogeikin, J. Shu, Ho.Mao, J. Z. Jiang, *Origin of Pressure-Induced Polyamorphism in* $Ce_{75}Al_{25}$ *Metallic Glass*, Phys. Rev. Lett. 104 (2010) 105702

62. Johansson, B. *Alpha-gamma transition in Cerium is a Mott transiti*on. Phil. Mag. 30 (1974) 69–482

63. L. Belhadi, F. Decremps, Pascarelli, L. Cormier, Y. Le Godec, Gorsse,F. Baudelet, Marini, and G. Garbarino. *Polyamorphism in cerium based bulk metallic glasses: Electronic and structural properties under pressure and temperature by x-ray absorption techniques*. Appl. Phys. Lett. 103 (2013) 111905

64. A. Lindemann, Ueber die Berechnung molekularer Eigenfrequenzen, Z Phys, 11 (1910), p. 609

65. W.H. Wang, P. Wen, Relation between glass transition temperature and Debye temperature in bulk metallic glasses, J Mater Res, 18 (2003), p. 2747

66. Xing-Qiu, Haiyang Niu, Dianzhong, Yiyi Li, Modeling hardness of polycrystalline materials and bulk metallic glasses, Intermetallics,19, 9, 2011, P 1275–1281

67. W. Voigt, Lehrbuch der KristaUphysik, B.B. Teubner, Leipzig (1928)

68. A. Reuss, Z. Angew. Mat. Mech., 9 (1929) 49

69. R. Hill, Proc. Phys. Soc. (London), 65 (1952) 349

70. Z. Zhang, R. Wang, L. Xia, B. Wei, D. Zhao, M. Pan, W. H. Wang, *Elastic behavior and microstructural characteristics of* $Nd_{60}Al_{10}Fe_{20}Co_{10}$ *bulk metallic glass investigated by ultrasonic measurement under pressure*. J. Phys.: Condens. Matter, 15 (2003) 4503

71. W. H. Wang, *Correlations between elastic moduli and properties in bulk metallic glasses*. J. Appl. Phys. 99 (2006) 093506

72. W. H. Wang, *Bulk Metallic Glasses with Functional Physical Properties*. Adv. Mater., 21 (2009) 4524

73. Y. Zhang, A. L. Greer, *Correlations for predicting plasticity or brittleness of metallic glasses.* J. Alloys Comp., 434 (2007) 2-5

74. B. Li, J. Kung, R. C. Liebermann, *Modern techniques in measuring elasticity of Earth materials at high pressure and high temperature using ultrasonic interferometry in conjunction with synchrotron X-radiation in multi-anvil apparatus,* Phys. Earth Planet. Inter., 143 (2004) 559-574